Quaternary Science Reviews 349 (2025) 109136

Contents lists available at ScienceDirect

Quaternary Science Reviews

journal homepage: www.elsevier.com/locate/quascirev

Coastal boulders emplaced by extreme wave events impacting the ABC islands (Aruba, Bonaire, Curaçao; Leeward Antilles, Caribbean)

Giovanni Scardino [a,b,*], Alessio Rovere [c,d], Chiara Barile [a], N.A.K. Nandasena [e], Denovan Chauveau [c], Malena Dahm [f], Patrick Boyden [d], Sonia Bejarano [g], Elisa Casella [c], Harold Kelly [h], Eric Mijts [i], Giovanni Scicchitano [a,b]

[a] Department of Earth and Geo-Environmental Sciences, University of Bari Aldo Moro, 70125, Bari, Italy
[b] Interdepartmental Research Center for Coastal Dynamics, University of Bari Aldo Moro, 70125, Bari, Italy
[c] Department of Environmental Sciences, Informatics and Statistics, Ca' Foscari University of Venice, Venezia, Italy
[d] MARUM, Center for Marine Environmental Sciences, University of Bremen, Bremen, Germany
[e] Civil and Environmental Engineering Department, United Arab Emirates University, Al Ain, 15551, United Arab Emirates
[f] Department of Biology and Chemistry, University of Bremen, Bremen, Germany
[g] Leibniz Centre for Tropical Marine Research (ZMT), Fahrenheitstraße 6, 28359 Bremen, Germany
[h] National Archaeological Museum Aruba, Oranjestad, Aruba
[i] University of Aruba, Oranjestad, Aruba

ARTICLE INFO

Handling editor: Claudio Latorre

Keywords:
Tsunami
Hurricane
Numerical models
Boulders
Radiocarbon ages

ABSTRACT

Large coastal boulders are ubiquitous geomorphological features that are emplaced along coasts by extreme marine events such as storms, hurricanes, and tsunamis. Many large coastal boulders have been identified on emergent fossil coral reefs on the windward sides of the Aruba, Bonaire, and Curaçao (ABC) islands in the Leeward Antilles of the Caribbean. Here, structure-from-motion/multi-view stereo techniques were used to map boulder sizes at several coastal sites in the ABC Islands as well as construct digital terrain models of the surrounding areas. Chronological constraints on boulder transport were established through the radiocarbon dating of the vermetids and coral colonies that comprised boulders located along a ridge on Aruba Island. A suite of hydrodynamic models was used to empirically derive the required flow thresholds for boulder displacement to determine whether tsunamis or hurricanes were responsible for detaching and transporting these boulders. Our results suggest that multiple tsunamis, most likely triggered by the El Pilar fault, located near the Venezuelan coast, were the cause of boulder detachment and transport in this region during the Holocene, between 4000 and 500 years BP.

1. Introduction

The impacts of extreme wave events are preserved in the geological record in several forms along the world's coastlines. In general, high-energy waves caused by extreme storms and tsunamis lead to the formation of out-of-size landforms as well as the deposition of out-of-place sediments (Nott, 2003a,b; Cox et al., 2020; Scardino et al., 2020 and references therein). These may occur as large coastal boulders (Nott, 2003a, 2003b; Nandasena et al., 2011b) or wide washover fans in backshore areas (Gianfreda et al., 2001; Vött et al., 2009; May et al., 2012). Several studies have investigated the scenarios that were most likely to be responsible for coastal boulder displacement in different regions around the globe (Mastronuzzi and Sansò, 2000; Nott, 2003a; Goto et al., 2010, 2011; Evelpidou et al., 2020; Pedoja et al., 2023). In general, the literature suggests that more cases of boulder mobilization can be attributed to large storms, such as (extra-)tropical cyclones (Cox et al., 2018; Hall, 2011; Hall et al., 2006; Scicchitano et al., 2020; Terry et al., 2016) , storm-induced energetic infragravity waves (Watanabe et al., 2023), or waterspouts (de Lange et al., 2006) than to tsunamis (Paris et al., 2010; Pignatelli et al., 2009; Scicchitano et al., 2007, 2012). .

Differentiating between tsunami- and storm-generated coastal landforms is challenging and, in the case of coastal boulders, is commonly resolved by applying empirical equations to determine the

* Corresponding author. Department of Earth and Geo-Environmental Sciences, University of Bari Aldo Moro, 70125, Bari, Italy.
E-mail address: giovanni.scardino@uniba.it (G. Scardino).

https://doi.org/10.1016/j.quascirev.2024.109136
Received 18 October 2024; Received in revised form 28 November 2024; Accepted 2 December 2024
Available online 11 December 2024

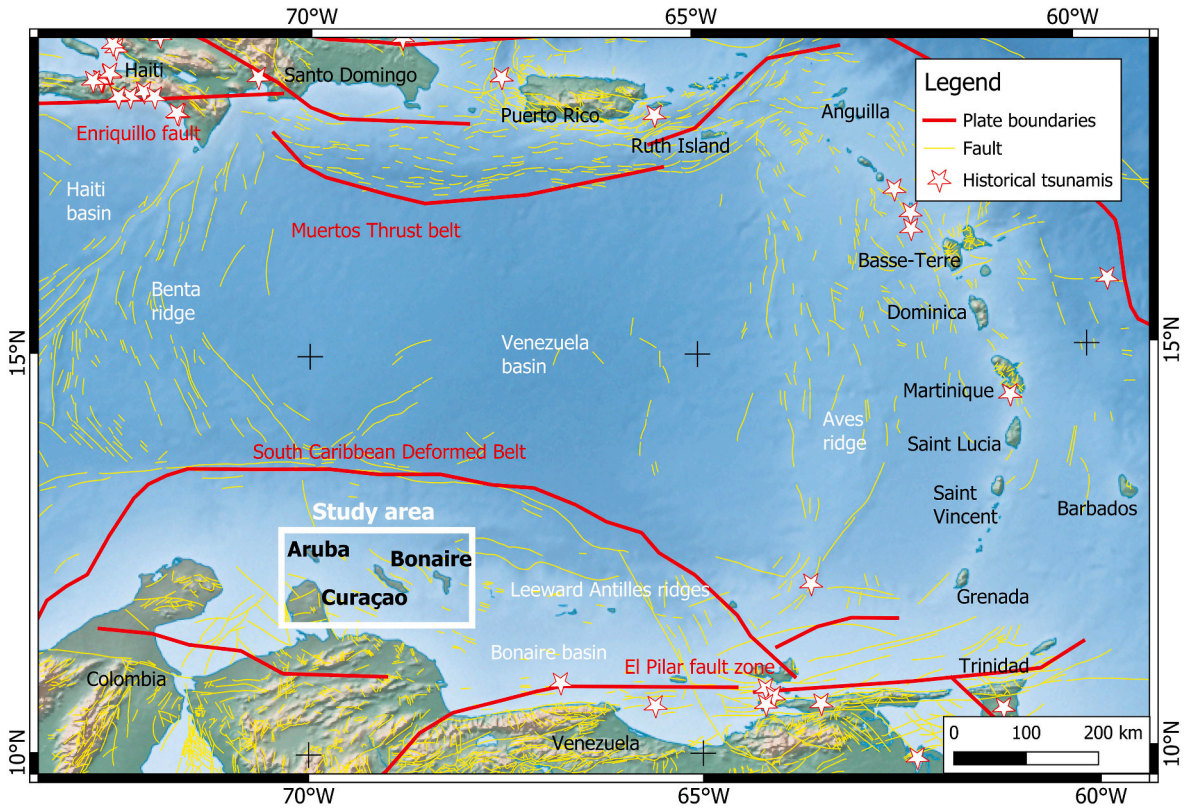

Fig. 1. The main study area in the context of the Lesser Antilles, including the main structural elements. The plate boundaries and fault structures follow French and Schenk (2004), and the locations of historical tsunami sources are obtained from Lander et al. (2002). The Aruba, Curaçao, and Bonaire (ABC) islands are highlighted in the white inset. Background map from Natural Earth Data (https://www.naturalearthdata.com/, accessed June 21, 2024).

minimum flow speed required to move the boulders observed at a given location (Nott, 2003a; Goto et al., 2009; Nandasena et al., 2011a, 2022; Weiss and Diplas, 2015; Roig-Munar et al., 2023). Despite the widespread application of this approach, distinguishing between the different types of extreme events responsible for boulder emplacement remains contentious(Weiss and Diplas, 2015; Cox et al., 2020; Roig--Munar et al., 2023; Dunán-Avila et al., 2024). Instrument records and eyewitness accounts of large boulder displacements provide a reliable basis for modeling extreme wave events (Scicchitano et al., 2020; Nandasena et al., 2022; Delle Rose, 2024). In addition, the reliability of the geological evidence can be improved by correlating it to historical sources (of known ages), which can provide additional details on the events and their effects (Delle Rose et al., 2020; Lario et al., 2020; Dewey et al., 2021). Furthermore, the integration of age constraints, such as radiocarbon dates, with numerical modeling can provide important insights into the extreme events that drive coastal boulder emplacement.

Here, we reviewed geological evidence of past extreme wave events recorded by coastal boulders on the Aruba, Curaçao, and Bonaire (ABC) islands of the Lesser Antilles (Caribbean). These boulders were likely emplaced by Holocene paleo-tsunamis and hurricanes (Scheffers, 2002; Scheffers and Kelletat, 2006); however, a consensus has yet to be reached on the origin and timing of these tsunamigenic events (Morton et al., 2008; Pignatelli et al., 2010; Watt et al., 2010; Engel and May 2012; Oetjen et al., 2015, 2020). To identify the most reliable source for these boulder displacements, we followed a forward modeling approach based on the dimensional features of the coastal boulders. We report new data on the geomorphological characteristics of the boulders and the surrounding rocky coasts, as well as new radiocarbon ages that provide constraints on the timing of boulder motion related to extreme wave events within the Holocene. We then compare the flow velocities obtained from our numerical models to the flow velocities calculated from empirical equations of incipient motion (Nandasena et al., 2022). In this way, we identify the most reliable sources of boulder displacement from both chronological data and the dynamics of extreme wave events.

2. Study area

The ABC islands are located on the Leeward Antilles ridge (Fig. 1), which was formed by Cretaceous–Cenozoic tectonic interactions between the Caribbean and South American plates (Avé Lallemant, 1997; Beardsley and Avé Lallemant, 2007). The ABC islands are characterized by stepped Quaternary coral reef terraces that flank older Cretaceous volcanic cores (e.g., Alexander, 1961; Fouke et al., 1996; Muhs et al., 2012). The lowest of these terraces contain well-preserved fossil corals dated to marine isotope stage (MIS) 5e (~122 ka ago, Fig. 2a) (Obert et al., 2016; Lorscheid et al., 2017). The MIS 5e terrace (which is, at places, incised by fluvial erosional channels known locally as *bokas*; Fig. 2b) terminates in sea cliffs that are fronted by a recent subtidal reef platform, which has been colonized by the vermetid *Petaloconchus* sp. (Hoeksema et al., 2022). Typical geomorphological imprints that can be observed on the rocky coasts of ABC Island include boulder ridges and ramparts (Scheffers, 2002; Scheffers et al., 2014).

Imbricated boulder ridge deposits and isolated coastal boulders frequently occur on the windward side of the ABC islands atop the MIS 5e terrace (Scheffers, 2002, 2004). These deposits are parallel to the coastline 20–250 m from the cliff front and primarily consist of well-rounded coral fragments from the recent subtidal reef (Scheffers, 2002; Radtke et al., 2003; Spiske et al., 2008; Engel and May 2012) or parts of the MIS 5e reef. In the Caribbean, similar ridges generally extend approximately 15 km alongshore, with crest heights ranging from 3 to 8 m above mean sea level (Morton et al., 2008). In many cases, the ridges are either not or only slightly asymmetric (Scheffers, 2002; Scheffers and Kelletat, 2006; Scheffers et al., 2014), with a steep seaward slope and a

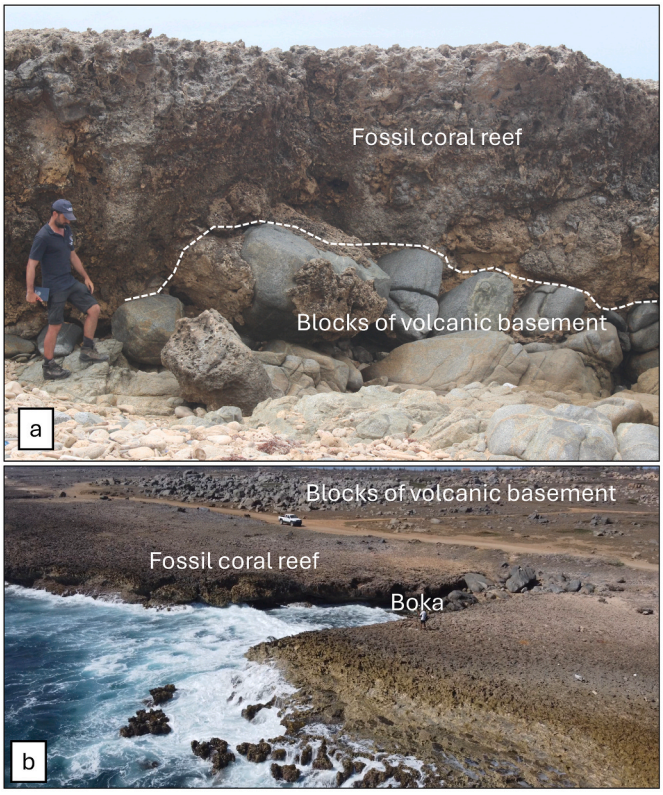

Fig. 2. Main geomorphological features found on the ABC islands: a) Contact between blocks of volcanic basement and fossil coral reef dated to the Late Pleistocene (MIS 5e), located in Aruba. b) Fossil coral reef terrace on the windward side of Aruba, incised locally by a fluvial erosional channel locally known as a *boka*.

gentle landward slope (Scheffers, 2005; Robinson et al., 2006; Morton et al., 2008). These ridges are irregularly punctuated by outsized coastal boulders that mostly occur at locations where the cliff front is near-vertical and the recent reef platform is relatively narrow (Focke, 1978; Scheffers, 2002; Pignatelli et al., 2010).

The ramparts consist of scattered, small-to medium-sized debris deposits with thicknesses ranging from decimeters to meters; these are generally located several meters from present-day coastlines or active cliff fronts and overlie a mildly sloping coast (Scheffers, 2002, 2004). Ramparts occur on both the leeward and windward sides of ABC Islands, with the most developed landforms observed in northeastern Curaçao and along the east-facing coastal stretch on Bonaire (Scheffers, 2002). They consist of debris and cobbles ranging from decimeters to around 1 m with a gently landward-sloping planar profile. These deposits are located up to 100 m inland from the coastline, at an elevation usually ranging from 6 to 10 m above sea level (asl), and become more scattered and thinner further inland (Scheffers, 2002; Scheffers et al., 2014).

2.1. Evidence of extreme waves on the ABC islands

The geomorphological records of the ABC Islands show that they have experienced various extreme storms and paleo-tsunamis (Table 1); these are particularly evidence in *bokas* and lagoonal areas (Engel et al., 2012a) as well as on the rocky coasts (Scheffers, 2002; Scheffers and Kelletat, 2006). Stratigraphic and geochemical data reported by Engel et al. (2012a), obtained through cores sampled from *bokas* and lagoons, revealed the occurrence of three main tsunami events that impacted the shores of these islands 3300, 2000, and 500 years before present (BP). Analyses of the boulders and some of the ridges atop the lower terrace of Bonaire revealed a sequence of extreme wave events that occurred between 4300 and 500 years BP (Scheffers, 2002, 2004, 2005; Scheffers et al., 2014). This broad sequence was identified through radiocarbon dating of vermetid reef and coral samples from the boulders (Scheffers, 2002). This sequence of events has been revised by other authors to

Table 1
Landforms that are evidence of extreme storms and paleo-tsunamis in the ABC islands. CE = Common Era, BP = Before Present, BCE = Before Common Era. References: 1—Scheffers, 2002; 2—Scheffers et al., 2009; 3 – Scheffers (2005); 4—Engel et al., 2012a; 5—Baptista et al., 1998; 6—Engel and May, 2012; 7—Harbitz et al., 2012; 8 – Engel et al., 2010; 9- Radtke et al. (2003); 10—Engel et al., 2012b; 11 - Rixhon et al., 2018; 12- Klosowska (2003).

Event (References)	Date	Dating method	Analyzed samples	Landforms and deposits	Location
Hurricane Lenny 1999 CE (1)	November 13, 1999 CE	–	*Acropora cerviconis*	Coral rubble spit	*Washikemba NP,* northwest Bonaire
Hurricane Tecla 1877 CE (2,3)	1877 CE	Radiocarbon, Electron-Spin- Resonance (ESR)		Ridge deposits	Salina Tarn, Bonaire
Tsunami 1755 CE (5,6)	November 1, 1755 CE				Great Antilles, Leeward Antilles
Tsunami 1530 CE (4,7,8)	1 September 1530 CE	Historical sources (4,7); Radiocarbon (8)	Vermetids	High-energy deposits	Lagun, Bonaire, ABC islands
Tsunami 500 BP (1,9)	1500 CE;	Radiocarbon	Vermetids, corals, gastropods	Rampart, ridges, boulders	ABC islands
Tropical cyclone 1000 BP (10)	950 CE	Radiocarbon	Gastropods	Normally graded strata separated by thin mud laminae	Salina Tarn, Bonaire
Tsunami 1500 BP (1)	400 CE	Radiocarbon	Vermetids, corals, gastropods	Rampart, ridges, boulders	ABC islands
Tsunami 1600 BP (8,11)	350 CE	Radiocarbon (8);^{230}Th/U (10),	Plant remains (8); Flowstone layer(10)	High-energy deposits (8); Boulders (10)	Lagun, Bonaire(8); Spelonk, Bonaire (10)
Tsunami 2000 BP (8)	50 BCE	Radiocarbon	Plant remains (8)	Sublittoral sediments interrupting onshore sedimentary sequences	Lagun, Boka Washikemba, Bonaire
Tsunami 3100 BP (8)	1850 BCE	Radiocarbon	Plants remain	High-energy deposits	Playa Grandi, Bonaire
Tsunami 3300 BP (4, 9, 12)	1350 BCE	Radiocarbon	Plant fragment, C. cancellate, Corbula sp.	High-energy deposits with peat clasts	Klein Bonaire, Salina Tarn, Boka Bartol, Bonaire(4); Druif, Aruba (9); St. Michiel lagoon, Curaçao (12)
Tsunami 3500 BP (1)	1550 BCE	Radiocarbon	Vermetids, corals, gastropods	Rampart, ridges, boulders	ABC islands
Tsunami 3600 BP (8)	1650 BCE	Radiocarbon	Gastropods	Two thin graded beds of 2 and 1 cm thickness	Klein Bonaire

Fig. 3. Boulders surveyed on the ABC Islands: a) boulder composed of vermetids in Aruba; b) sampling of a boulder composed of *Diploria* sp. that was transported from a recent reef platform to the top of the MIS 5e terrace in Aruba; c) sampling of a boulder composed of vermetids along the ridge in northwest Aruba.

account for the effects of long-term coastal processes and hurricanes that may have moved the coastal boulders following their initial emplacement (Morton et al., 2006, 2008; Spiske et al., 2008).

The Caribbean region has been impacted by multiple tsunamis, as evidenced by historical accounts dating back to the 16th century (Lander et al., 2002). These tsunamis were caused by either earthquakes or non-seismic geologic events (e.g., volcanic eruptions, flank collapses, and submarine landslides). The largest recorded earthquake in the Caribbean was a magnitude 7.5–8 event between Guadeloupe and Antigua in 1843 (Bernard and Lambert, 1988). Only two trans-oceanic tsunami events have been reported in the Caribbean: the 1755 Lisbon earthquake (November 1st, 1755; Baptista et al., 1998; O'Loughlin and Lander, 2003) and the 1761 Lisbon earthquake (March 31st, 1761; O'Loughlin and Lander, 2003). A total of 65 earthquake-generated tsunamis have been reported by the National Geophysical Data Center (NGDC, 2021), the largest of which occurred on November 18th, 1867 after a strong MS 7.5 earthquake in the Virgin Islands (Zahibo and Pelinovsky, 2001).

An important tsunamigenic source close to the ABC islands is the El Pilar fault zone, a right-lateral strike-slip fault located offshore Venezuela, which accommodates most of the relative motion between the Caribbean and South American plates (Perez et al., 2018). The El Pilar fault structure has been responsible for several tsunamis, including events in 1530 and 1853, which were likely associated with offshore ruptures of this fault (Audemard, 2007). The kinematics of the El Pilar fault zone have been inferred from geodetic measurements published by Jouanne et al. (2011). Following the Haiti earthquake on January 12th, 2010 (Calais et al., 1998), the area was impacted by two tsunamis, one caused by the combined movement of a submarine landslide in the north of Haiti (Fritz et al., 2013) and the other generated by the displacement of the North Hispaniola and Enriquillo faults that cross-cut the island of Haiti (Pararas-Carayannis, 2010; Poupardin et al., 2020).

There are currently 12 active volcanoes located across 10 major islands throughout the Lesser Antilles. Volcanic flank collapses in this area have triggered several tsunamis (Boudon et al., 2007). In 1939, the Kick'em Jenny volcanic eruption caused a series of tsunami-like waves with amplitudes of around 2 m in the Grenadines and Grenada Islands (Smith and Shepherd, 1993a, 1993b). It should be noted that tsunamis generated by a submarine landslide generally propagate radially away from the slide, while tsunamis generated by fault displacement typically propagate with crests parallel to the fault rupture (Harbitz et al., 2006, 2014). The largest submarine landslide that occurred near the ABC Islands was associated with the active margin of northern Colombia, another potential tsunamigenic source for the central Caribbean basin (Leslie and Mann, 2016).

In contrast to the relative rarity of tsunamis in the Caribbean, approximately 1000 tropical storms and around 200 hurricanes impacted this region in the past century (Scheffers et al., 2009; NHC-NOAA, 2024). Hurricane genesis generally begins above the Atlantic Ocean waters; the hurricanes then move westward across the Windward Islands, over the Caribbean Sea, and finally turn northwest. Hurricane Lenny in 1999 remains the only hurricane to date that formed within the Caribbean Sea and tracked east–northeast (Bries et al., 2004). In the Lesser Antilles, Curaçao was hit by a minor hurricane on September 23rd, 1877, which damaged infrastructure and deposited coral rubble (Spiske et al., 2008). More recently, Hurricane Ivan (September 7th, 2004) hit the ABC Islands causing significant structural damage to houses and other infrastructure; the greatest damage and heaviest rainfall was reported on Aruba (Scheffers and Scheffers, 2006).

3. Materials and methods

This study adopts a workflow consisting of three main steps: i) geomorphological mapping of areas characterized by coastal boulders, including three-dimensional (3D) mapping of the largest boulders; ii) collecting samples of smaller boulders composed entirely of vermetids and corals emplaced along the ridges for radiocarbon dating (Fig. 3); and iii) running a suite of hydrodynamic models (Delft3D-Celeris-XBeach models) to compare the flow velocities required to displace the boulders—as calculated from empirical equations—with those generated by historical extreme wave events that have impacted the ABC Islands.

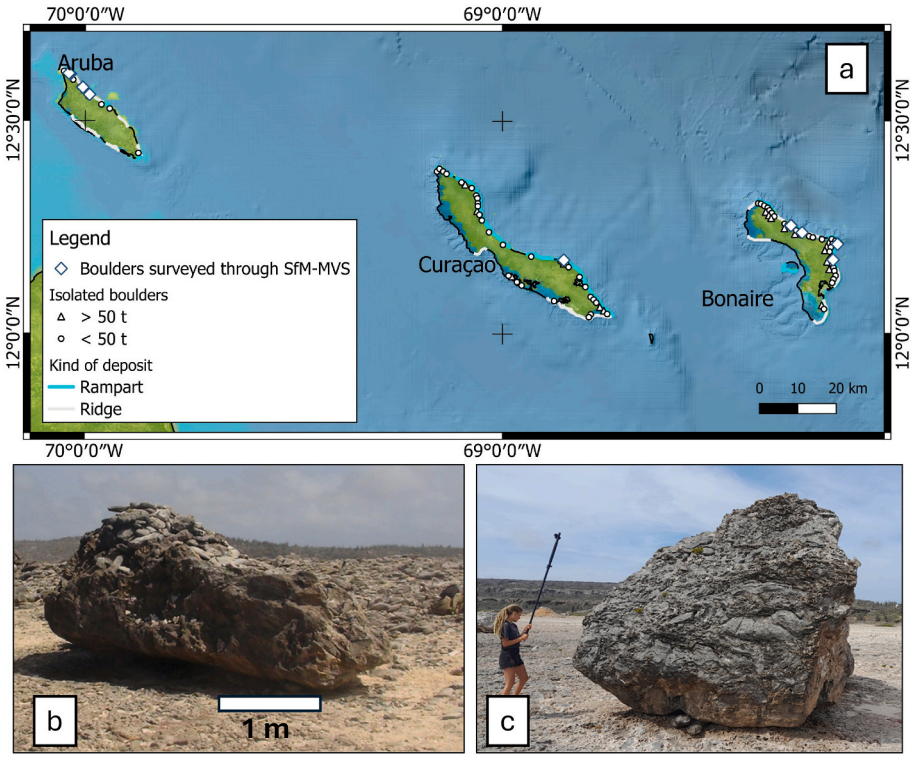

Fig. 4. a) Map showing the areas of the ABC islands that are characterized by boulder ridges or isolated boulders as reported in the literature (blue lines, Scheffers, 2002; Engel et al., 2012a). Boulders surveyed through close-range SfM/MVS in this study are represented using white diamonds; b) an example of a displaced boulder sitting on top of ridge deposits at South Ranchero Curason (Aruba); c) land-based SfM/MVS performed on a boulder in Boka Onima on Bonaire.

Fig. 5. Rocky coastlines surveyed by unmanned aerial systems (UAS) for the reconstruction of digital elevation models. a) Map showing locations of the areas surveyed using UAS. b) Boulder ridge deposits in Tierra del Sol. c) Boulder ridge deposits in South Ranchero Curason.

Geomorphological mapping was conducted using land-based structure-from-motion (SfM)/multi-view-stereo (MVS) methods to reconstruct the 3D features of boulders on the ABC Islands (Fig. 4). Morpho-topographic surveys were also performed at two sites in Aruba, henceforth referred to as "*Tierra del Sol*", and "*South Ranchero Curason*" (Fig. 5a). These two sites are characterized by large coastal boulders associated with ridge deposits. The date of the events related to boulder displacements was constrained by the radiocarbon dating of the biological materials that comprise the coastal boulders, which were composed of either vermetids or corals. To account for sea level changes at the time of boulder transport, we used local relative sea levels reconstructed from glacial isostatic adjustment models (ICE-7G) (Roy and Peltier, 2015, 2017, 2018). Empirical equations describing the incipient motion of these boulders were then applied to determine the minimum flow velocity required to displace these boulders based on their size and mass (Nandasena et al., 2022). Finally, hydrodynamic models of different tsunamis and hurricanes were used to reproduce the wave propagation, flow depth, and cross-shore velocity associated with these events. These results were compared with incipient modes to determine the most likely series of extreme wave events responsible for the boulder displacements.

3.1. Boulder surveys on the ABC islands

Land-based SfM/MVS methods were used to calculate the dimensions of the coastal boulders. Photos of each boulder were acquired at a distance of less than 10 m using a Sony DSC-RX100M3 camera (8.8 mm focal length; 5472 × 3648 resolution). Coded ground control points (GCPs) were measured using an EMLID RS2+ differential GNSS receiver. GCP measurements were corrected in post-processing. Scale bars were used during the SfM/MVS process to scale and optimize the model. Two kinds of base stations were used during post-processing: i) GNSS stations from NOAA Continuously Operating Reference Stations (CORS) located at Aruba and Curaçao (IDs CN19 and CN40); ii) an EMLID RS2+ base

station that was installed in Bonaire during previous surveys. The collected ellipsoid elevations were converted into geodetic elevations referenced to Earth Gravitational Model 2008; Pavlis et al. (2012).

The photos and GCPs were processed in the Agisoft Metashape Professional (v.2.0.2) software to reconstruct 3D polygonal models for each boulder. Point clouds were extracted for each boulder and imported into the CloudCompare software (v.2.13.1). We then extrapolated the "ab" and "ac" surfaces following the approach described by Nandasena et al. (2022). The surfaces were converted to meshes and translated to planar projections to determine their areas and axial lengths ($a > b > c$). Finally, the true volumes of each boulder were calculated in CloudCompare. Bulk densities were calculated by correlating the lithotype and coral species comprising each boulder and the associated density values reported in Spiske et al. (2008) for the same lithotype. Boulder weights were then calculated by multiplying each boulder's volume by its bulk density.

Additionally, the largest boulders in Aruba were associated with an extended ridge deposit. Analogous ridge deposits have also been observed in Curaçao and Bonaire. Here, the boulders with *a*-axes greater than 0.5 m were mapped using a GoPro HERO Black11 camera (24.4 mm focal length and 5599 × 4927 resolution) and the same dGNSS positioning described above.

3.2. Radiocarbon dating

To provide chronological constraints on the timing of the formation of the boulder ridges, we collected 10 samples (weighing 100 g each) from the boulders composed of vermetids and two additional boulder samples. These samples were then analyzed using a single-stage accelerator mass spectrometer (SSAMS, NEC, USA) and AGE-3 Automated Graphitization Equipment (Ionplus AG, Zürich). The analysis was performed by the Vilnius Radiocarbon Lab (Center for Physical Sciences and Technology, Vilnius, Lithuania). Conventional ^{14}C ages were calibrated in the Calib software (v8.20, Stuiver and Reimer, 1993; Stuiver et al., 2021) using the Marine20 curve and a ΔR value of −308 ± 29 yr, as reported by DiNapoli et al. (2021) for Aruba.

3.3. Morpho-topographic surveys and bathymetric data

To model extreme wave events on the ABC islands, we combined the digital elevation model (DEM) obtained from the Tandem-X mission (12-m resolution and vertical accuracy of 1 m; Uuemaa et al., 2020) with multibeam echo sounder (MBES) bathymetry data collected by the Dutch Ministry of Defense around the ABC islands (Dutch Caribbean, 2019). We then downsampled the data to match the GEBCO dataset (10-m resolution) and combined the two datasets. This allowed us to extend the DEM further offshore, allowing for the effective simulation of wave propagation for each modeled scenario. Aerial SfM/MVS methods were performed using a DJI Mini unmanned aerial system (UAS; 24 mm focal length and 8064 × 6048 resolution) at two locations: Tierra del Sol and South Ranchero Curason (Fig. 5). The UAS was flown at a height of 30 m above ground level and flight speed of ~2 m/s. Targets that were clearly visible in the UAS images and located along the cliff top were measured using GPS. The photos acquired by the UAS were processed following the same SfM/MVS workflow detailed in Section 3.1 to produce orthomosaics and georeferenced DEMs of the two areas with a cell resolution of 0.3 × 0.3 m.

To reconstruct the paleo-sea-level scenarios for extreme wave events, we utilized the ICE 7G glacio-isostatic model and compared it with field-based curves for Curaçao (Khan et al., 2017) and Bonaire (Engel et al., 2014).

The reconstructed cliffs in the two areas were modified based on the relative sea-level scenarios obtained from the ICE 7G curve, which assumes a radially symmetric viscosity profile for the Earth's mantle referred to as VM6 (Roy and Peltier, 2017). Specifically, it assumes that the viscosity of the upper mantle—located between the base of the lithosphere and the base of the transition zone at 660 km depth—is equal to 0.45 × 10^{21} Pa s. The chronological constraints obtained from radiocarbon dating were used to obtain the relative sea-level positions from the ICE 7G curve at different times. Isolines corresponding to the past sea-level positions were reported on the DEMs of Tierra del Sol to identify the position of the cliff base, assuming that a coral reef paleo-landscape also existed in the past. The DEMs were then modified in Surfer (v. 11.0), with the cliff slope extended seaward toward the past sea-level position to reconstruct the paleo-topography at the time of the extreme wave events corresponding to the annexed ridge deposits on the cliff top.

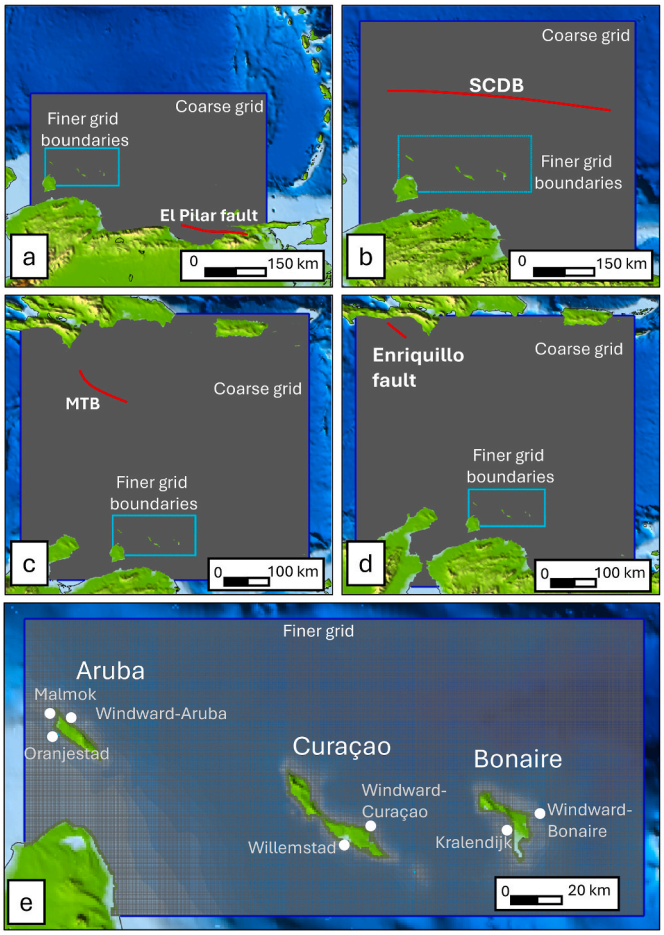

Fig. 6. Modeling grid for the Caribbean region built in Delft Dashboard. a) Coarse grid used for the El Pilar earthquake-generated tsunami; b) coarse grid used for the South Caribbean Deformed Belt (SCDB) earthquake-generated tsunami; c) coarse grid used for the Muertos Thrust Belt (MTB) earthquake-generated tsunami; d) coarse grid used for the Enriquillo earthquake-generated tsunami; e) finer grid used to extract water levels from time series data at the given locations.

3.4. Water level and wave modeling

Three potential sources of the extreme waves that impacted the coasts of the ABC islands were considered: i) earthquake-generated tsunamis, ii) landslide-generated tsunamis, and iii) tropical cyclones. Wave propagation modeling of the tsunami and storm events was performed at two different spatial scales (Fig. 6), with coarse grids used offshore (500 × 500 m) and a finer grid used in the study area, closer to the ABC Islands (80 × 80 m).

The boundary conditions of offshore wave propagation for earthquake-generated tsunamis were set using the Delft Dashboard toolbox, which was then passed into a Delft3DFlow and Delft3DWave

Table 2
Tsunamigenic sources and hurricane events considered for wave propagation modeling in the Lesser Antilles. References: 1—Brink et al. (2020); 2—Schubert, 1994; 3—Colón et al., 2015; 4—Pousse Beltran et al., 2016; 5- (Brink et al., 2008); 6—Boudon et al., 2007; 7—Lindsay et al., 2005; 8—Boudon et al., 1984; 9—Le Friant et al., 2003; 10—Dondin et al., 2012; 11—Joint Typhoon Warning Center (JTWC); National Hurricane Center (NHC); Unisys Weather.

Earthquake-generated tsunami							
Name of structure (references)	Length (km)	Strike	Dip	Width (km)	Focal depth (km)	Slip	Mw
Enriquillo faults, Haiti (1)	60	132°	84°	20	15.5	−2.6 m left-lateral 1.8 m reverse	7.1
EI Pilar fault zone, Venezuela (2,3,4)	270	88°	87°	20	15	1.6 m	7.7
South Caribbean Deformed Belt (SCDB) (5)	550	74.5°	17°	100	10	7.8 m	8.5
Muertos Thrust Belt (MTB) (5)	188	92.1°	10°	61	24 km	3 m	7.8

Subaerial landslide-generated tsunamis						
Name of landslide (references)	Length (km)	Thickness (m)	Density (kg/m^3)	Width (km)	Volume (km^3)	Age
Debris avalanche, Santa Lucia (6,7)	6	100	3100	5		39 ky BCE, 1760 CE
Soufriere (8,9)	1.5	200	3100	4	2	3100 BCE
Kick'em, Jenny (7,10)	6	20	2000	3.5	4.4	From 1939 to 2001 CE

Tropical cyclones			
Name of hurricane	Date	Mean sea-level pressure (hPa)	Wind speed (km/h)
Hurricane Cesar (11)	24 July—06 August 1996	945	215
Hurricane Ivan (11)	2–24 September 2004	910	210
Hurricane Felix (11)	31 August—5 September 2007	929	280
Hurricane Matthew (11)	28 September—9 October 2016	934	270

models (Le Quéré et al., 2020). Delft3D is a 3D coupled hydrodynamic numerical model that solves nonlinear shallow water equations on a staggered 3D grid using a finite difference scheme. The fault parameters and magnitude of the seismic event must be defined in the Delft Dashboard tsunami toolbox to generate the initial wave conditions. The fault parameters used in this study were derived from two main earthquake-generating seismic structures in Haiti and Venezuela that had previously impacted the Lesser Antilles in the last century (Table 2). The tsunamis were modeled using fault parameters obtained from marine geophysical campaigns reported by Brink et al. (2020).

Three significant landslide bodies were considered for landslide-generated tsunami wave propagation, which was conducted using a Boussinesq-type Geowave model (Watts and Tappin, 2012). The first landslide-generated tsunami model was based on the chaotic mass flow deposit associated with a horseshoe-shaped structure near offshore St. Lucia (Mattioli, 1995). A second landslide-generated tsunami was associated with the magmatic eruption of the Soufriere Hills that occurred at 3.1 ka BP (Boudon et al., 1984; Le Friant et al., 2003). Finally, the main volcanogenic tsunami threat is represented by the active submarine Kick'em Jenny volcano (northwest of Grenada), which is particularly prone to future collapse based on monitoring measurements (Smith and Shepherd, 1993b; Lindsay et al., 2005; Dondin et al., 2012).

The impact of storm waves on the ABC island was modeled in Delft3D by hindcasting the four main hurricanes that impacted the Lesser Antilles in the past 30 years. Simulations were performed in Delft3D Flow coupled with Delft3D Wave. Among the studied events, Hurricane Ivan (September 2004) had the strongest effect on the ABC Islands; its track passed 130 km north of the study area and affected the windward sides of the islands, with the strongest effects felt northwest of Aruba (Engel and May 2012). This event featured a peak flow depth of 1.5 m at the cliff's edge, with a flow velocity ranging from 5 to 7 m/s (Scheffers, 2005; Scheffers and Scheffers, 2006).

Wave propagation in the nearshore areas was performed on a finer grid using the Boussinesq model within the Celeris software (grid size 5 × 5 m) to assess coastal inundation (Tavakkol and Lynett, 2017, 2020). For each event, waves were resolved using the JONSWAP spectrum and characterized by the root-mean-square wave height and common peak period. These parameters were defined from the Delft 3D outputs at the coarse-grid boundaries. The relative sea level was also included in the model based on the outputs of the ICE-7G model (Roy and Peltier, 2015, 2017, 2018) after comparison with field-based sea-level curves (Engel et al., 2014; Khan et al., 2017).

To model the non-linear evolution of the wave field, we performed 1D simulations using the non-hydrostatic XBeach module. These simulations use a bed profile, tide conditions, and wave spectra as input parameters. The bed profiles were extracted from the bathymetric and morpho-topographic data for each island, using the coastal stretch in which the largest boulders were identified. These areas were chosen to simulate the cross-shore velocity in areas impacted by the highest waves. The tide conditions were assumed to be constant for the entirety of the simulation and were referenced from their respective paleo-relative sea-level datum. The same wave spectrum used for the Boussinesq model was also used in the XBeach-1D simulation.

Table 3
Coefficients used to calculate the minimum flow velocity required to transport boulders.

Coefficient	Value	Reference
Drag	1.5	Nandasena et al. (2022)
Lift—submerged/sub-aerial boulders and joint-bounded blocks	0.7	Nandasena et al. (2022)
Lift—cliff-edge blocks	2.0–2.7	Rovere et al., 2017
Static friction	0.177	Field data

3.5. *Threshold flow for boulder transport*

The boulder displacement caused by a wave's impact is determined by a matrix of forces and moments applied to the boulder when the water hits its surface. As the wave impacts the boulder, drag and lift forces act to move the boulder, while reduced-gravity forces (i.e., boulder mass minus buoyant force) and frictional forces resist motion. To assess the minimum flow velocity required to move each of the surveyed boulders in the study area, we applied the incipient-motion formula developed by Nandasena et al. (2022). Three different initial conditions (i.e., pre-transport boulder positions) were considered following the approach reported in Nandasena et al. (2011a, 2011b): i) subaerial/submerged, ii) joint-bounded, and iii) cliff-edge. For subaerial/submerged boulders, the three types of incipient transport modes are i) sliding, ii) rolling/overturning, and iii) saltation/lifting. Boulders starting from initial cliff-edge conditions may be transported by rolling/overturning and saltation/lifting, while joint-bounded boulders can only be lifted from their socket before the wave impact (Nandasena et al., 2013). Previously published coefficients were used for all incipient-motion calculations (Table 3). The static friction was determined by applying the approach described by Pollyea and Fairley (2012)

Table 4
Dimensional features of the studied boulders as obtained from close-range SfM/MVS analyses; densities were obtained through the correlation between lithotype/coral species and Archimedean buoyancy measurements reported in Spiske et al. (2008).

Boulder ID	Location	Lat. (N)	Lon. (E)	Elevation (m asl)	a-axis (m)	b-axis (m)	c-axis (m)	Projected ab (m^2)	Projected ac (m^2)	Volume (m^3)	Lithotype/corals species	Bulk density (kg/m^3)	Mass (tons)	Distance from the surf zone (m)
Ar1	*Aruba (South*	12.5615	−69.9895	4.60	3.26	2.28	1.75	6.24	5.03	12.186	*Acropora* sp. and rudstone matrix	2290	29	32
Ar2	*Ranchero Curason*	12.5616	−69.9898	5.80	2.17	1.82	1.56	2.59	2.70	3.507	*Acropora* sp. and rudstone matrix	2290	8.35	55
Ar3		12.5615	−69.9898	5.80	2.68	1.98	1.62	3.31	2.78	5.198	*Acropora* sp.	2290	12.37	55
Ar4		12.5787	−70.0062	4.50	4.56	2.59	2.12	8.12	6.28	12.845	*Acropora* sp.	2290	30.57	41
Ar5		12.5784	−70.0059	4.90	2.00	1.82	0.58	3.47	0.87	1.262	Serpulid reef rock	1770	1.77	38
Ar6	*Aruba (Tierra del*	12.6102	−70.0363	4.26	2.67	1.811	1.6	4.26	1.56	2.216	*Acropora* sp. and *Orbicella* sp.	2290	5.27	28
Ar7	*Sol)*	12.6103	−70.0364	3.80	2.57	1.56	0.98	3.8	2.22	2.620	*Acropora* sp. and rudstone matrix	2290	6.24	25
Ar8		12.6099	−70.0357	4.46	3.07	2.3	1.16	4.46	3.11	2.990	*Acropora* sp. and rudstone matrix	2290	7.39	30
Ar9		12.6101	−70.0366	4.15	2.01	0.95	0.72	1.84	1.2	0.416	Biocalcarenite	2720	0.99	51
Ar10		12.6099	−70.0360	4.15	1.51	0.66	0.62	0.67	0.74	0.220	Biocalcarenite	2720	0.53	52
Ar11		12.6114	−70.0391	3.80	2.21	1.69	1.15	2.52	1.77	1.416	*Acropora* sp.	2290	3.37	16
Ar12		12.6114	−70.0391	3.80	2.07	1.2	1.15	1.99	1.81	1.145	*Acropora* sp.	2290	2.73	16
Ar13		12.6114	−70.0394	3.20	2.52	1.28	0.38	3.20	0.92	0.640	Serpulid reef rock	1770	1.02	48
Cu1	*Curaçao*	12.1737	−68.8530	4.8	7.73	2.65	1.77	16.05	10.86	18.09	Biocalcarenite	2720	43.24	47
Bo1	*Bonaire (Boka*	12.2529	−68.3106	4.70	6.76	4.48	4.47	13.91	19.43	50.753	*Acropora* sp.	2290	120.79	150
Bo2	*Onima)*	12.2533	−68.3089	5.00	6.41	4.10	3.75	15.37	16.39	52.611	*Acropora* sp.	2290	125.21	52
Bo3		12.2531	−68.3094	5.40	4.59	4.47	3.03	14.60	9.46	40.247	*Acropora* sp.	2290	95.79	96
Bo4	*Bonaire (Arawak/ Boka Oliva)*	12.2374	−68.2825	7.10	7.94	5.15	5.14	33.12	20.28	79.943	*Acropora* sp. and rudstone matrix +10% *A. cervicornis* and rudstone matrix	2290	175.08	50
Bo5	*Bonaire*	12.2109	−68.1972	6.50	3.35	1.78	1.00	4.13	2.63	3.476	*Acropora* sp. and rudstone matrix	2290	8.59	24
Bo6	*(Lighthouse)*	12.2100	−68.1977	6.80	4.16	4.02	1.77	13.63	6.04	15.054	*Diploria* sp. and rudstone matrix	1040	37.18	51
Bo7	*Bonaire (Washikemba)*	12.1732	−68.2086	6.00	4.36	3.46	2.36	7.65	5.52	16.993	Biocalcarenite	2720	45.97	85

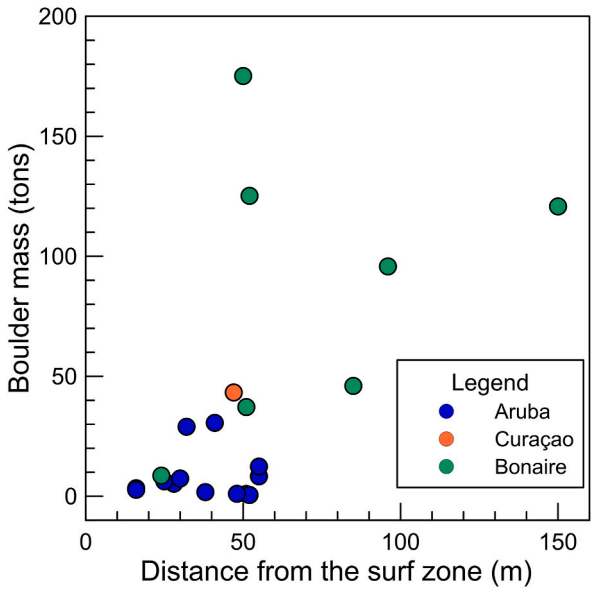

Fig. 7. Plot showing the relationship between distance from the surf zone (*x*-axis) and mass of the surveyed boulders on the three islands (*y*-axis).

on the point clouds obtained from SfM/MVS techniques.

4. Results

4.1. Size and minimum flow thresholds for coastal boulders

A total of 21 boulders were mapped using SfM/MVS (13 in Aruba, seven in Bonaire, and one in Curaçao). The surveyed boulders were composed of Pleistocene reef calcarenite and biocalcarenites and varied between 0.5 and 175 tons. The boulders were located at variable distances from the coast, ranging between 16 and 250 m from the shoreline, and at elevations between ~3 and ~7 m above present sea level (Table 4). In general, the boulders in Bonaire were larger, heavier, and were located farther from the coast than those observed in Curaçao and Aruba (Fig. 7). This observation provides some initial evidence that the boulders in Bonaire would have required more energy to transport compared to those in Curaçao and Aruba, irrespective of the mode of transport under consideration (Fig. 8). In Bonaire, the flow required to initiate boulder movement—regardless of the mode of transport—was 5.72 ± 3.46 m/s on average (1-sigma). The equivalent value for Aruba was 3.47 ± 1.8 m/s (1-sigma), while the only boulder we measured in Curaçao would have required an average flow velocity of 5.02 ± 1.09 m/s (1-sigma). Higher minimum flow velocities are required for the saltation/lifting mode in subaerial and submerged conditions, for lifting in joint-bounded conditions, and for rolling in cliff-edge conditions (see Fig. 9).

4.2. Chronological constraints on boulder motion

The boulders surveyed using SfM/MVS were composed of Pleistocene reef limestone; no biological remains could be attributed to organisms that died during transportation, which would potentially provide a hard constraint on the timing of the displacement event. Consequently, the next best proxy was the age of the boulder ridge, which comprises smaller boulders of Holocene corals (*Diploria* sp. and *Orbicella* sp.) and vermetids (*Petaloconchus* sp.). These were likely transported from subtidal environments (for corals) or the intertidal area (for vermetids) to the top of the MIS 5e reef terrace. Sampling was performed in the two areas surveyed by UAS: eight samples were collected in Tierra del Sol, while two samples were collected from South Ranchero Curason. The dates obtained from these samples were correlated with the eight large boulders that were sampled from Tierra del Sol and used in the flow velocity assessment.

The age distribution of the boulders within the ridge at Tierra del Sol and South Ranchero Curason shows that the ridges are polycyclic, with the boulders being emplaced within the last 4000 years (Table 5) by different extreme events during relative sea-level rise driven by glacial isostatic adjustment processes (Fig. 10). Only one boulder dates back to ~7 ka BP; this boulder was emplaced with a relative sea level several

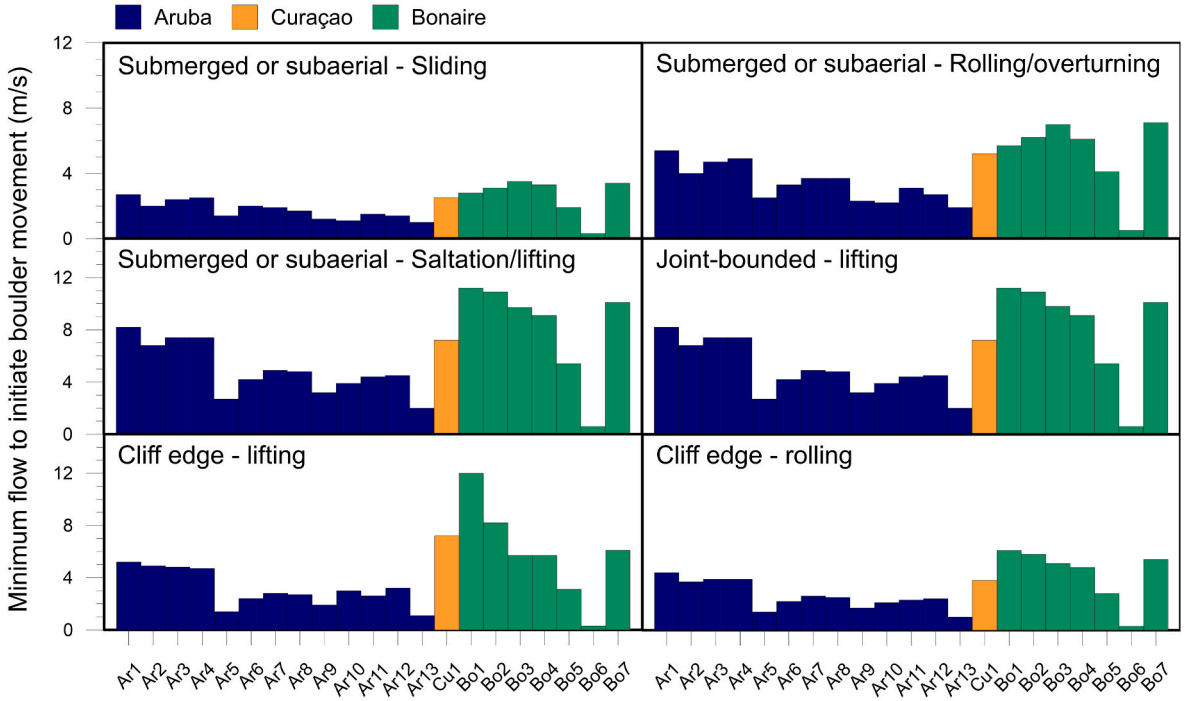

Fig. 8. Minimum flow velocity required to initiate boulder displacement for different pre-transport scenarios as calculated following the empirical equations reported in Nandasena et al. (2022). More details can be found in the Supplementary Information.

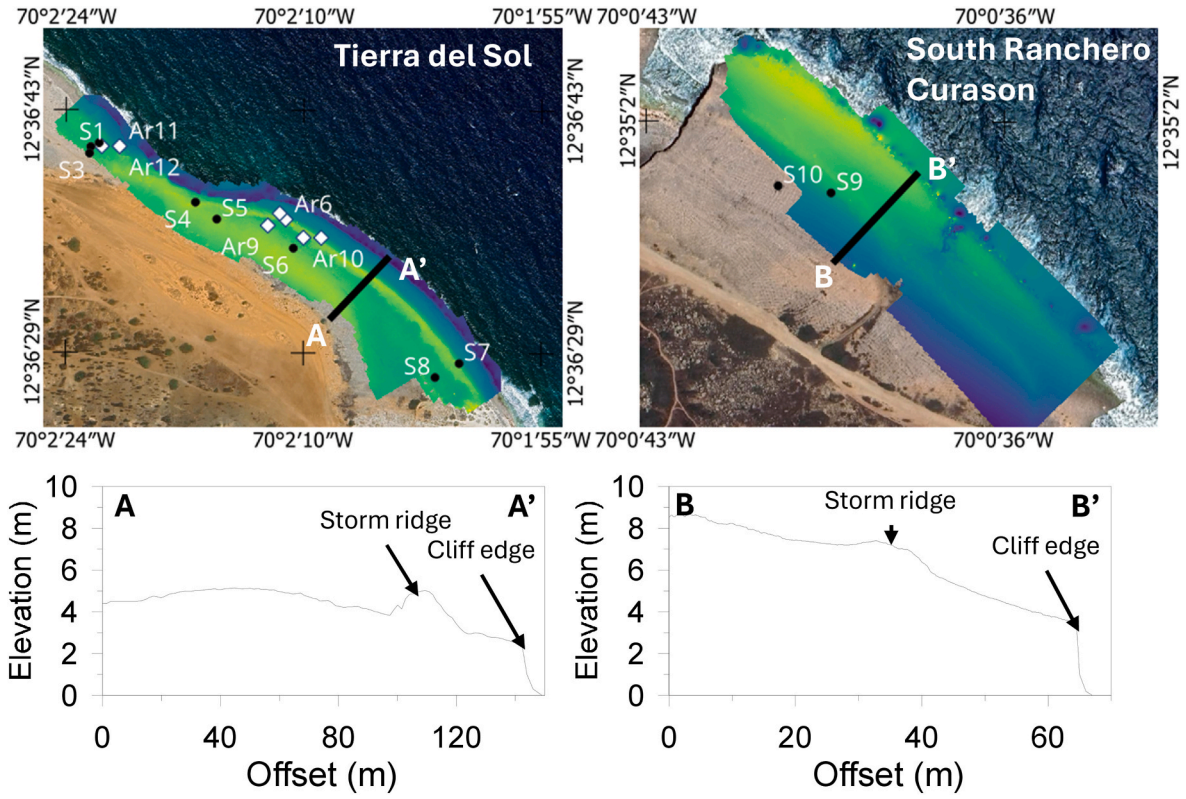

Fig. 9. DEMs obtained from SfM-MVS in Tierra del Sol and South Ranchero Curason. The locations of the boulder samples are presented as black dots, while the boulders processed for flow assessment are shown as white diamonds. The profiles show the cliff elevations and storm ridge locations.

Table 5
Location and radiocarbon ages obtained from the vermetid and coral boulders that comprise the boulder ridge at Tierra del Sol and South Ranchero Curason. CE = Common Era; BCE = Before Common Era.

ID	LAB CODES	Latitude	Longitude	Dated material	Age (years BP)	pMC	Calibrated age 95.4%	Calibrated age 99.4%	Age (cal years BP, 2-sigma)
S1	FTMC-HW32-1	12.611456	−70.039446	*Petaloconchus* sp.	2161 ± 27	76.42 ± 0.26	84 BCE–83 CE	167 BCE–163 CE	1948 ± 165
S2	FTMC-HW32-2	12.611391	−70.039586	*Petaloconchus* sp.	1995 ± 27	78.01 ± 0.26	124 CE–286 CE	50 CE–373 CE	1742 ± 81
S3	FTMC-HW32-3	12.611283	−70.039606	*Petaloconchus* sp.	3623 ± 29	63.70 ± 0.23	1876 BCE–1703 BCE	1959 BCE– 1612 BCE	3741 ± 173
S4	FTMC-HW32-4	12.610480	−70.037820	*Petaloconchus* sp.	1522 ± 27	82.74 ± 0.28	658 CE–785 CE	602 CE–871 CE	1226 ± 135
S5	FTMC-HW32-5	12.610201	−70.037460	*Petaloconchus* sp.	3875 ± 28	61.73 ± 0.22	2206 BCE–2023 BCE	2304 BCE–1937 BCE	4072 ± 184
S6	FTMC-HW32-6	12.609726	−70.036168	*Diploria* sp.	3004 ± 28	68.80 ± 0.24	1108 BCE–931 BCE	1201 BCE–854 BCE	2975 ± 174
S7	FTMC-HW32-7	12.607833	−70.033370	*Petaloconchus* sp.	937 ± 28	88.99 ± 0.31	1257 CE–1382 CE	1187 CE–1429 CE	641 ± 121
S8	FTMC-HW32-8	12.607601	−70.033775	*Orbicella* sp.	4192 ± 30	59.34 ± 0.22	2630 BCE–2451 BCE	2745 BCE–2356 BCE	4493 ± 195
S9	FTMC-HW32-9	12.583610	−70.010970	*Petaloconchus* sp.	4521 ± 29	56.96 ± 0.21	3035 BCE–2870 BCE	3162 BCE–2780 BCE	4909 ± 191
S10	FTMC-HW32-10	12.583648	−70.011266	*Petaloconchus* sp.	6730 ± 31	43.27 ± 0.17	5468 BCE–5331 BCE	5541 BCE–5252 BCE	7350 ± 145

meters lower than the present day.

As the relative sea-level position at the time of boulder transport influences onshore wave propagation, we used two different paleo relative sea-level scenarios during the modeling; these were derived from the glacial isostatic adjustment models shown in Fig. 10, which show a gradual increase in the relative sea level starting from −2.35 m (4500 years BP) to −0.26 m (500 years BP) (Fig. 11a). This shift in Holocene sea-level would have significantly changed the position of the cliff and reef platform (Fig. 11 b–c), with a coastline located farther out to sea than its present-day position. Assuming the same relative sea-level scenario for the fringing reef during the Holocene, the DEM obtained from the aerial SfM/MVS method on Aruba was merged with bathymetric data and corrected using the two different cliff positions that corresponded to the 500 years BP and 4000 years BP scenarios, respectively (Fig. 11):

- cliff base located at −0.26 m, with a coastline displacement toward the sea of 25 ± 5 m (scenario for 500 years BP)

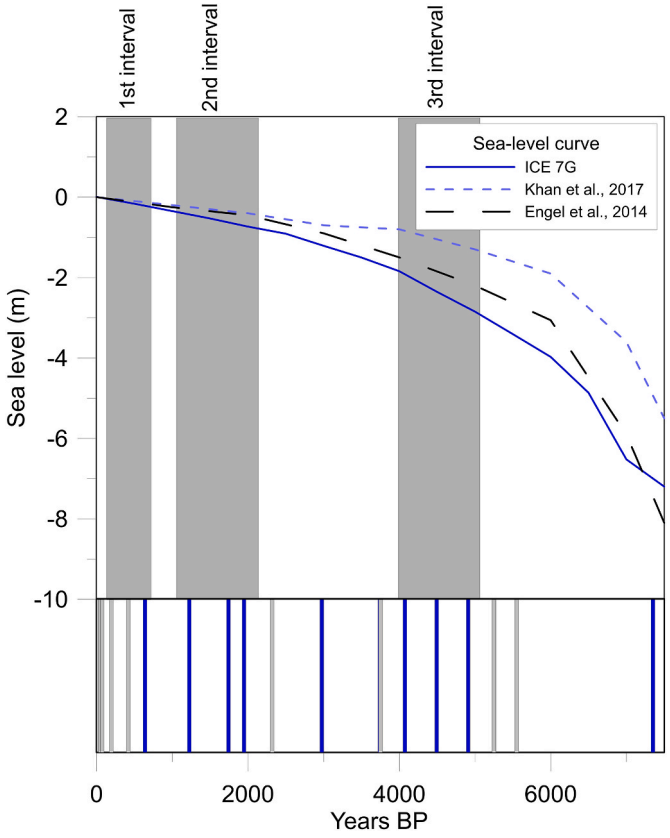

Fig. 10. Relative sea level resulting from glacial isostatic adjustment processes in the ABC islands. Intervals with tsunami events are reported in gray boxes. The lower part of the graph shows the average ages of boulders dated in this work (blue lines; Table 5) and the occurrence of tsunamis that impacted the ABC islands as reported in other studies (gray lines; Table 1).

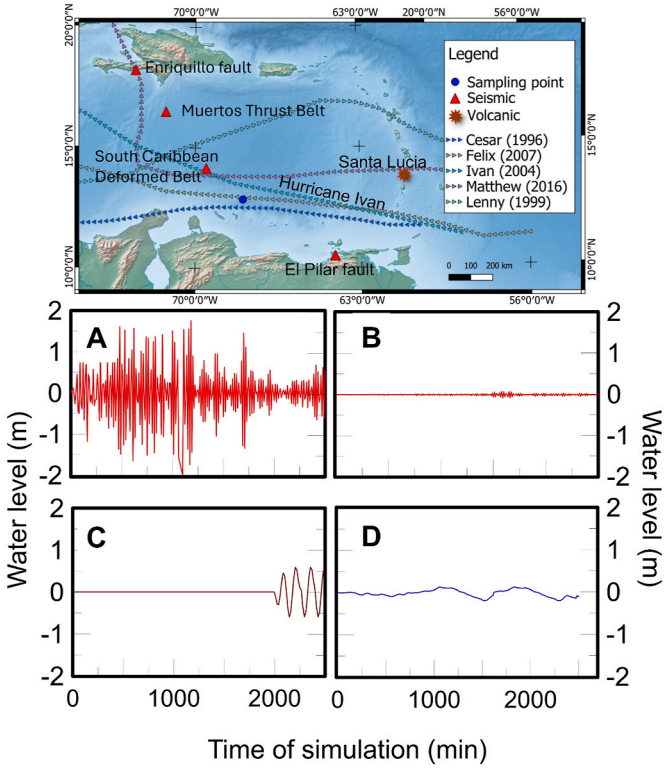

Fig. 12. Water levels for different extreme wave events modeled in the Caribbean region: a) El Pilar fault-generated tsunami, b) Enriquillo fault-generated tsunami, c) tsunami generated by the flank collapse of the Santa Lucia volcano, and d) storm surge modeled in response to Hurricane Ivan (September 2004).

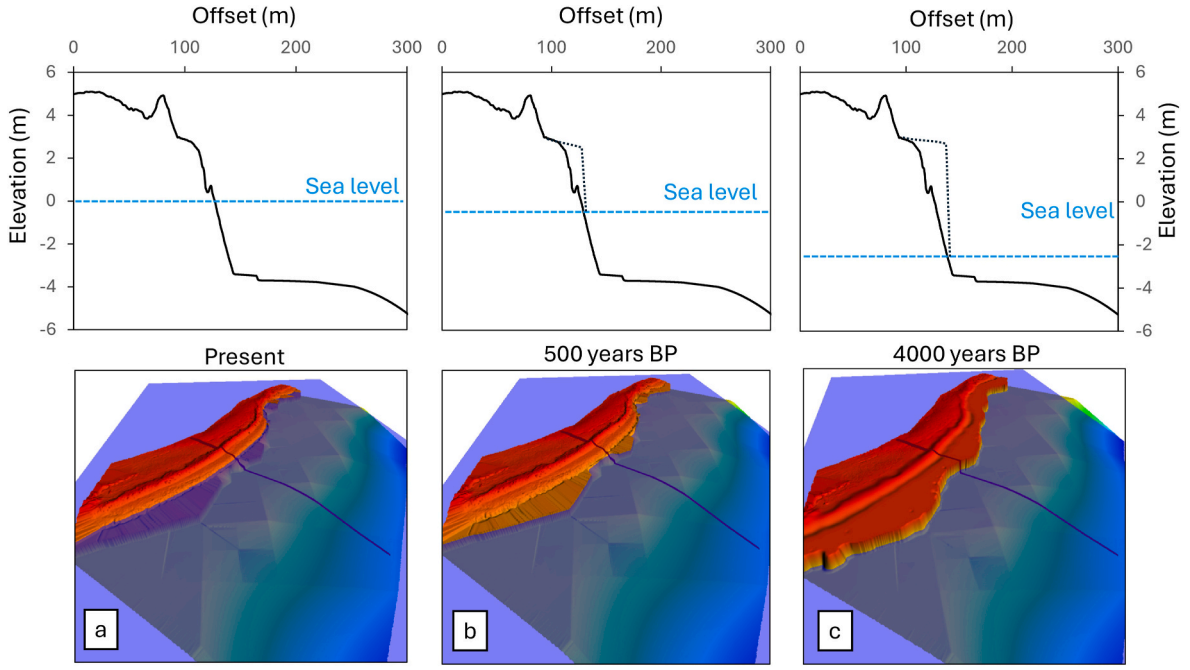

Fig. 11. Reconstruction of topography from the DEMs obtained from UAS surveying at Tierra del Sol (Aruba island): a) DEM of the current sea-level position, b) DEM with the coastline at −0.26 m (500 years BP), and c) DEM with the coastline at −1.65 m relative to the DEM in 11b (4000 years BP).

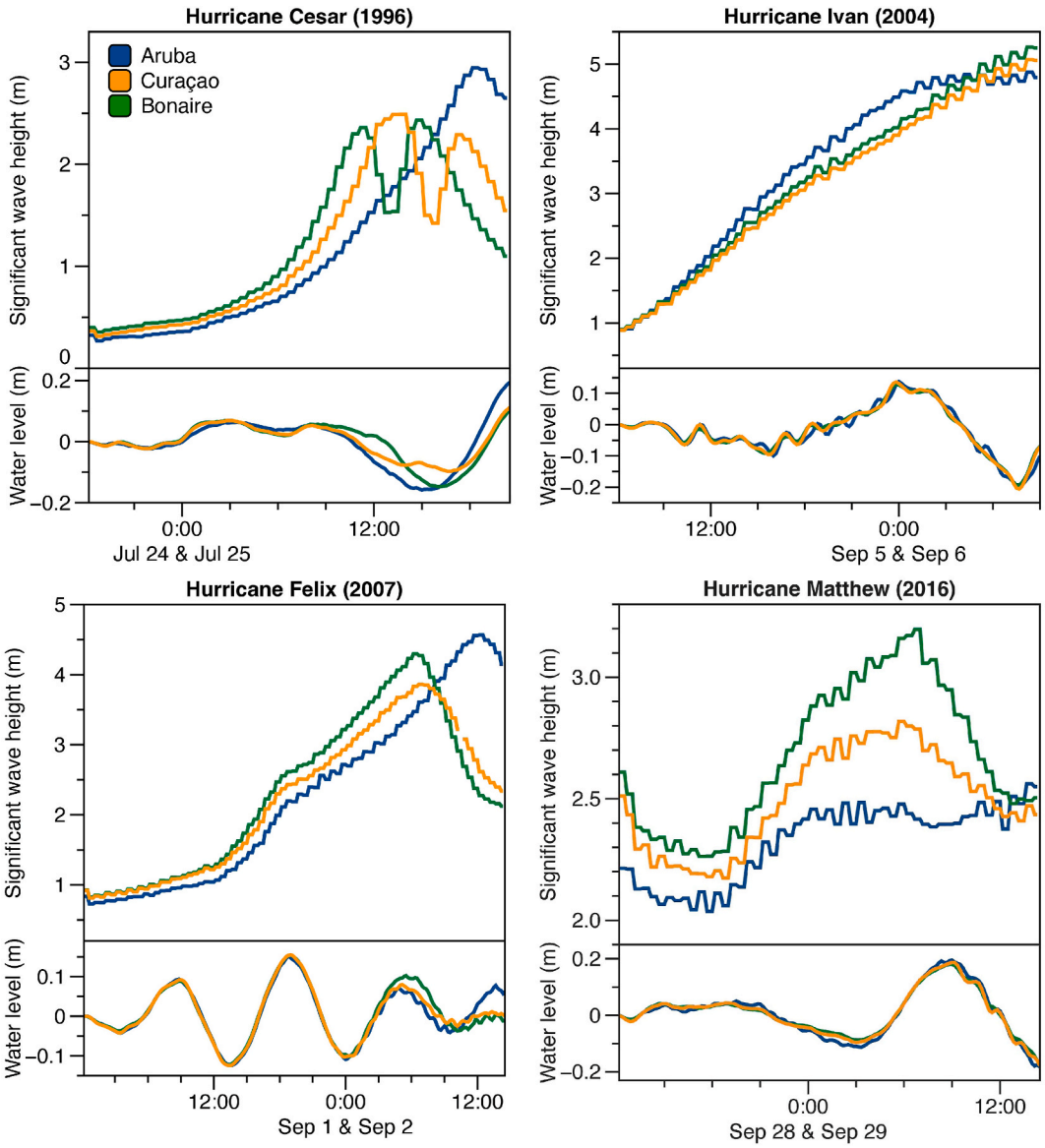

Fig. 13. Water level and significant wave height modeled for the main hurricanes that impacted the ABC Islands (events are described in Table 3, while sampling points are reported in Fig. 12).

- cliff base located at −1.65 m, with a coastline displacement toward the sea of 62 ± 5 m (scenario for 4000 years BP)

4.3. Modeling of extreme wave events

Mesoscale wave propagation modeling provides insights into the nature of the waves that could have emplaced the surveyed boulders in the ABC islands. While the models for landslide-generated tsunamis caused by volcanic flank collapses indicated that these waves would have completely dissipation over the Aves ridge (eastern Caribbean), the modeled earthquake-triggered tsunamis produced high water levels on the windward side of the ABC islands, where the boulders were emplaced. Of the two fault systems modeled in this study, the Haiti-sourced seismogenic tsunami produced very low water levels, while the seismogenic tsunami driven by slip along the El Pilar fault resulted in high water levels (Fig. 12). The models indicate that the activation of this fault system triggers a westward-propagating wave that results in high water levels on both the leeward and windward sides of the ABC Islands.

In terms of hurricanes, Hurricane Ivan (2004) resulted in the displacement of coastal boulders weighing up to 2.5 tons in Bonaire (Bries et al., 2004; Scheffers and Scheffers, 2006; Engel et al., 2012b). However, although the path of this hurricane crossed the Caribbean region approximately 140 km north of the ABC Islands, it generated swell waves that were amplified by cliff fronts, reaching heights of around 12 m on the windward side of Bonaire (Scheffers and Scheffers, 2006). Our model of these events indicates that the ABC Islands were impacted by water levels of about 0.15 m asl, with significant wave heights of 6 m (Fig. 13). Another major event that impacted the ABC Islands was Hurricane Felix (2007), whose predicted water level and significant wave height values were 0.15 m and 4.5 m, respectively. Simulations of Hurricane Cesar (1996) and Hurricane Matthew (2016) exhibited water levels of about 0.2 m and wave heights of around 3 m along the coast of ABC Islands.

Among the modeled extreme events, the highest water levels along the coasts of the ABC islands were generated by tsunamis triggered by the El Pilar fault and the South Caribbean Deformed Belt (SCDB) structures. The estimated first arrival times from the tsunami generated by the El Pilar earthquake were 50 min in Bonaire, 60 min in Curaçao, and 80 min in Aruba (after the initialization of the simulation).

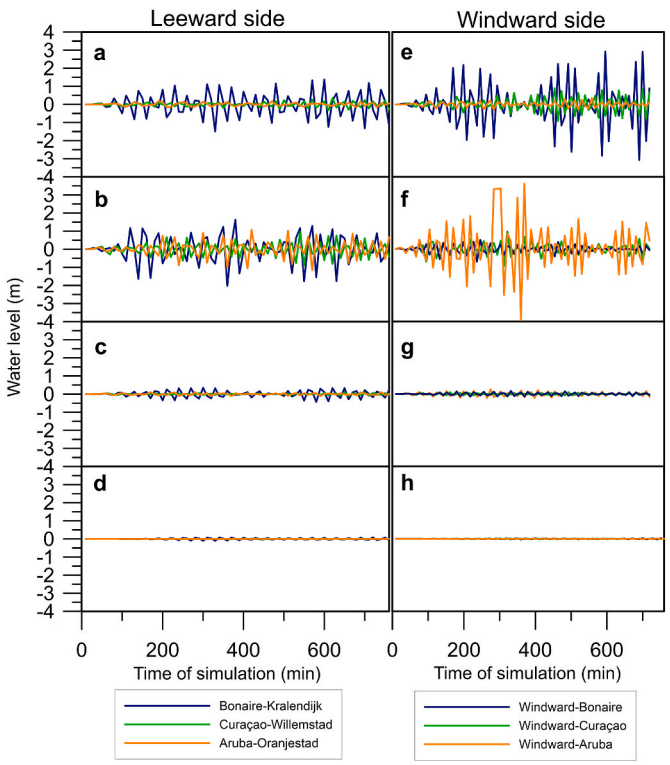

Fig. 14. Time series of the modeled earthquake-generated tsunamis. Water levels of the leeward side of the ABC islands as modeled for the a) El Pilar, b) SCDB, c) MTB, and d) Enriquillo faults; water levels of the windward side of the ABC islands as modeled for the e) El Pilar, f) SCDB, g) MTB, and h) Enriquillo faults.

However, the estimated first arrival times from the tsunami generated by the SCDB structure were 20 min in Aruba, 30 min in Curaçao, and 80 min in Bonaire. Furthermore, the raised water levels produced by the tsunami generated by the El Pilar fault were observed to dissipate as they progressed towards Aruba, with higher water levels (~3 m) modeled in Bonaire that became progressively lower in Aruba and Curaçao (~1m; Fig. 14a–e). In contrast, tsunamis generated by the SCDB structure exhibited higher water levels in Aruba (~4.3 m) compared to Curaçao and Bonaire (~0.8 m; Fig. 14b–f). Water levels observed in models of the Enriquillo fault and Muertos Thrust Belt (MTB) structures exhibited values lower than 0.5 m (Fig. 14c–h).

4.4. Cross-shore velocity modeled in XBeach 1D

A 1D non-hydrostatic XBeach model was used to calculate the flow velocity generated by the highest tsunami waves shown in Fig. 14. The water level and cross-shore velocities were extracted along each transect reported based on the non-linear wave field modeled in XBeach 1D (Fig. 15). The results show an increased cross-shore velocity at the edge of the cliff, with values exceeding the flow velocity threshold needed to initiate boulder transport. The maximum cross-shore velocities in the 500 years BP and 4000 years BP scenarios were approximately 7.5 m/s on Aruba, 8 m/s on Curacao, and 12 m/s on Bonaire. The highest water levels occurred in the 500 years BP scenario, ranging from 5 to 7 m. These values could strengthen the hypothesis of a tsunami impact capable of moving the observed boulders, as these values are greater than the c-axis values of the surveyed boulders.

5. Discussions

5.1. Limitations on the minimum flow for extreme wave scenarios

The distribution of coastal boulders in the ABC Islands provides a clear indication of the impact of extreme wave events capable of dislodging the boulders. Boulders weighing more than 50 tons are found only in Bonaire and Curaçao, with the largest ones located on the western side of Bonaire (Scheffers, 2002; Scheffers et al., 2014), indicating that the minimum flow required to initiate boulder movements was higher in Bonaire than in Curaçao and Aruba. The inverse modeling presented in this study shows that tsunamigenic sources located in the eastern part of the Caribbean basin—such as the El Pilar fault—are most likely to have caused boulder displacement. The strongest swells were also associated with storms arriving from the eastern side of the Caribbean basin. In contrast, several other probable sources could be responsible for boulder displacements that may have impacted from other directions, including the SCDB structure located offshore on the northern side of the ABC Islands (Brink et al., 2008; UNESCO, 2012). Considering the minimum flow velocities reported in Fig. 8, a singular marine event is not capable of transporting boulders more than 100 m (Goto et al., 2010; Nandasena et al., 2011a). Flows measured in similar conditions during the 2011 Great East Japan tsunami showed that boulder displacements exceeding 100 m require flow velocities of 7.5–23.7 m/s (Nandasena et al., 2013); consequently, based on the geographic context of the ABC islands, it is more realistic to consider multiple wave events that may have contributed to the observed cumulative different boulder displacements.

It should be noted that some criticisms have been leveled against the application of the incipient motion formula to distinguish types of wave events responsible for boulder movements in the ABC Islands (Engel and May 2012; Costa et al., 2021). In particular, the wave energy can be underestimated if the pre-transport setting and transport mode are not clearly defined. For example, the boulders of Boka Olivia (Bonaire) have their a-axis sub-parallel to the coastline, suggesting a saltation transport mode (Watt et al., 2010). However, evidence of detachment surfaces and notches on the boulders can provide additional insights into their transport mode (Pignatelli et al., 2010; Engel and May 2012); a comparison between the transport mode and minimum flow required to initiate boulder movement is reported in Table 6 based on the field evidence reported in Engel and May (2012).

Boulder Bo4 is the largest boulder surveyed in this study and overlies a 0.7 m high pedestal, indicating a long period of protection from solution agents on the order of many hundreds or even thousands of years (Engel and May 2012). There is a notch at the base of Bo4, suggesting that the most likely pre-transport setting is that of a joint-bounded emplacement. Furthermore, Bo4 is the heaviest boulder recorded in this study, and the minimum flow required for its displacement is a useful benchmark for the application of the inverse modeling approach. Indeed, the modeled cross-shore velocities were higher than those indicated by the incipient mode for both the 4000 years BP and 500 years BP scenarios.

5.2. Attribution of the most reliable tsunamigenic source

Chronological constraints were obtained from the radiocarbon dating of subtidal and intertidal samples transported onto the MIS 5e terraces of Aruba island. The calibrated ages revealed three key horizons during which multiple wave events would have been capable of dislodging the boulders of ABC Islands: 500, 2000, and 4000 years BP. The 500 years BP horizon is consistent with other geological evidence of a tsunami that occurred on September 1st, 1530, such as debris avalanches into the sea of the eastern Islands (i.e., Basse-Terre, Guadeloupe, St. Lucia, Grenada) (Boudon et al., 1984, 2007) and fine-grained extreme wave deposits on the lagoonal areas of Lesser Antilles (Engel et al., 2012a; Engel and May 2012).

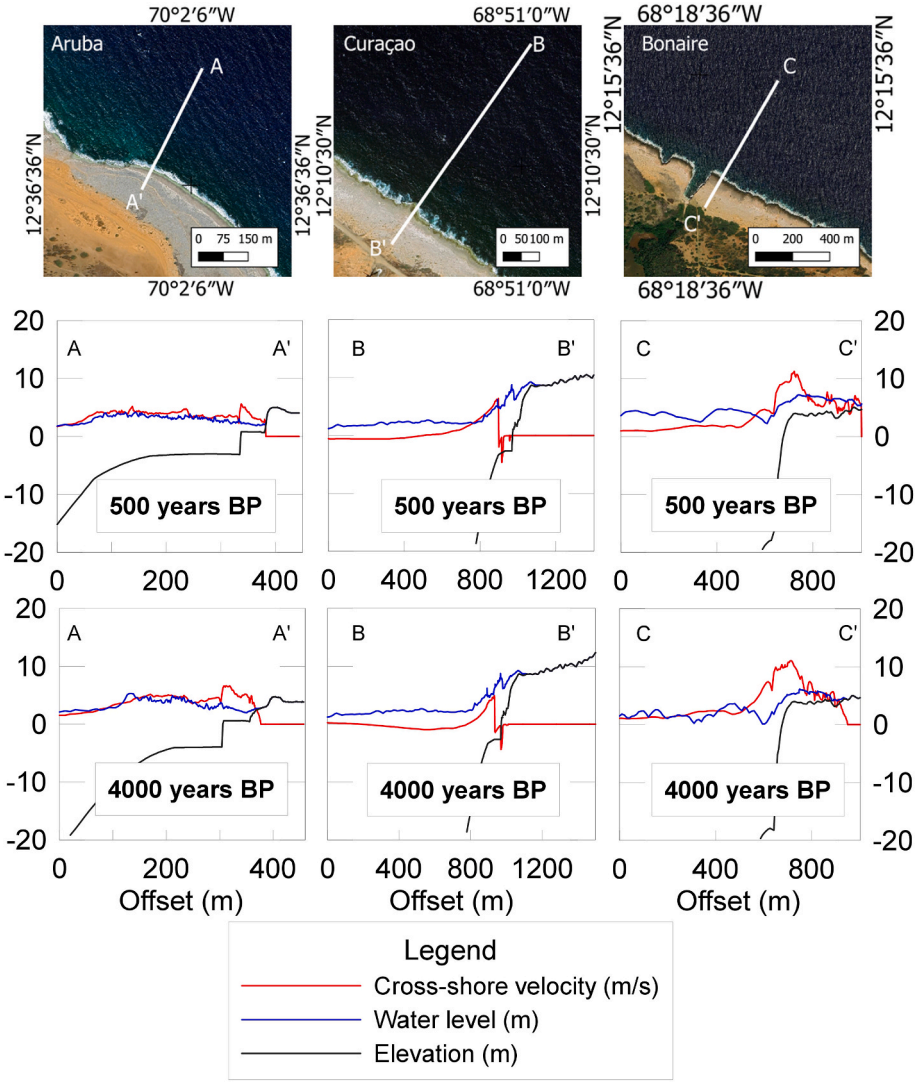

Fig. 15. Non-hydrostatic simulation outputs obtained through the XBeach model of the ABC islands. The different times were extracted from the calibrated ages, while the topographic profiles were extracted from the paleo-landscape of the relevant sea-level scenarios.

Table 6
Pre-transport settings of the surveyed boulders as well as the correlation between their masses and the minimum flow velocities required to initiate boulder movements as calculated from the equations described in Nandasena et al. (2022).

ID boulder	Pre-transport setting	Transport mode	Location	Event	Mass (t)	Minimum flow required to initiate boulder displacement (m/s)	Modeled cross-shore velocities (m/s)
Bo2	Cliff-edge boulder	Cliff edge - Rolling/overturning (Rixhon et al., 2018)	Boka Onima	Tsunami 1200 BP	125.21	8.2	12
Bo5	Joint-bounded	Cliff edge - Rolling/overturning (Rixhon et al., 2018)	Spelonk Lighthouse	Tsunami 1200 BP	8.59	5.4	
Bo4	Joint-bounded	Cliff edge - Rolling/overturning (Engel and May, 2012b); Saltation (Watt et al., 2010)	Boka Olivia	–	175.08	9.1	

The current positions of the coastal boulders suggest that they were displaced by more than 100 m from the surf zone. This degree of movement could not have occurred during a single event as indicated by the cross-shore velocities predicted by the XBeach 1D model (Nandasena et al., 2011a, 2013; Cox et al., 2020). Therefore, boulder transport must have occurred across multiple events as indicated by the chronological ranges obtained from the radiocarbon dating (Table 5). The initial displacement of coastal boulders could have occurred during the 4000 years BP scenario, during which the maximum cross-shore velocity reached 12 m/s (Fig. 11). This velocity is consistent with other tsunamis that have caused the displacements of similar boulders, as observed during events such as the 2004 Indian Ocean Tsunami (Paris et al., 2010; Nandasena et al., 2011a).

Field evidence from Spain has shown that minimum flow velocities between 3.6 and 8 m/s can displace coastal boulders by a maximum distance of 40 m (Lario et al., 2023). Similarly, boulders weighing 60–90 tons were moved up to 32 m by wave flows of around 10 m/s in New South Wales, Australia (Young et al., 1996). Several instances of coastal

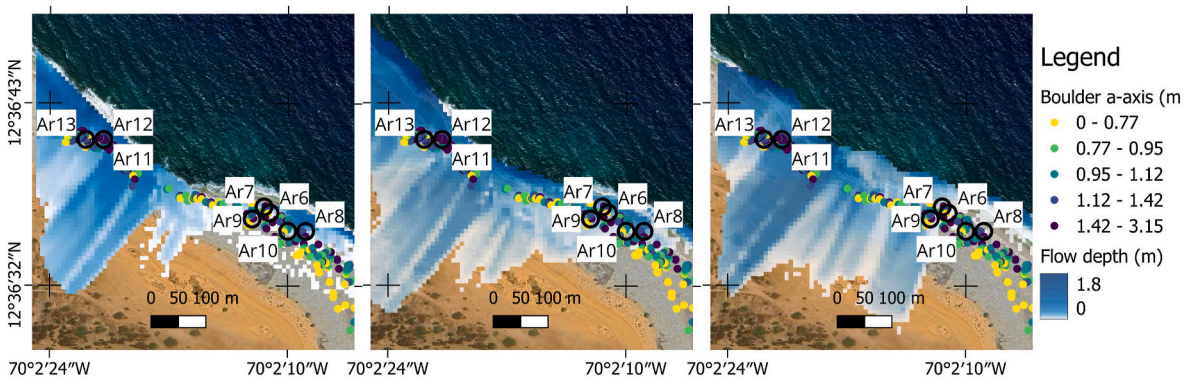

Fig. 16. Modeled inundation scenarios at the Tierra del Sol site, Aruba: a) inundation caused by Hurricane Ivan (2004) at present-day sea levels, b) inundation caused by the El Pilar tsunami based on relative sea-levels in the 500 years BP and c) 4000 years BP scenario. The empty black circles indicate the location of the mega-boulders surveyed at this site, while the colored dots represent smaller boulders that comprise the ridge, colored by their a-axis size as measured from field photos. Basemap source: Esri, Maxar, Earthstar Geographics, and the GIS User Community.

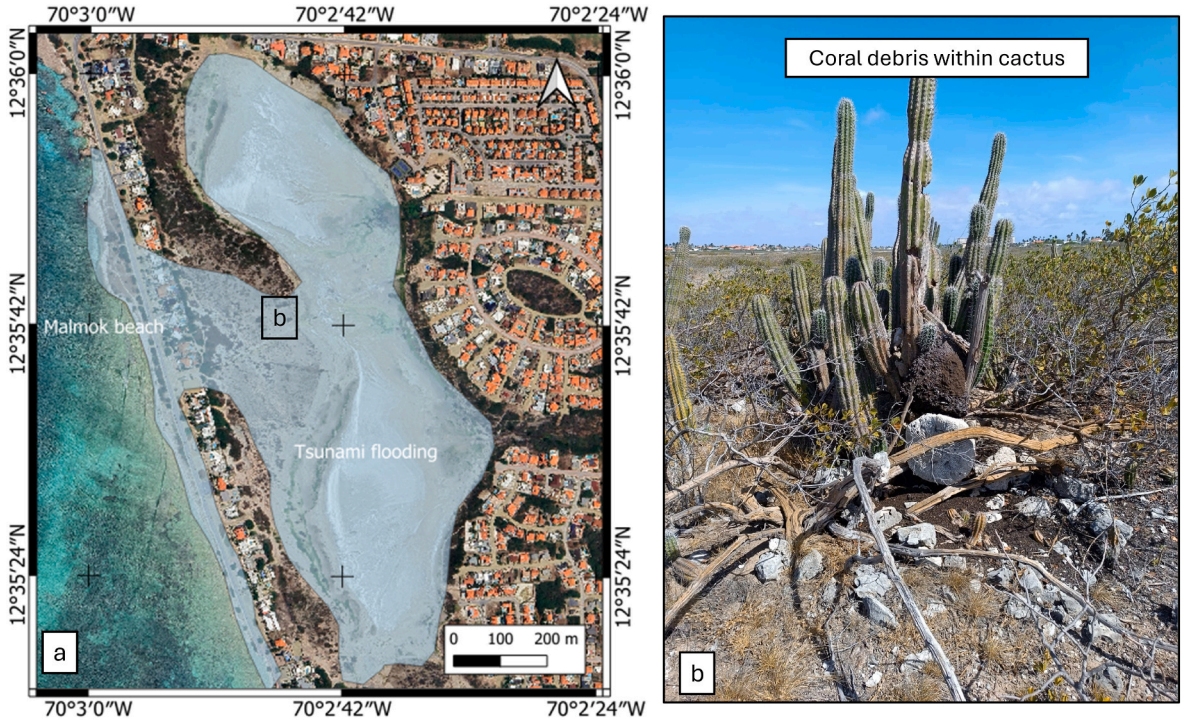

Fig. 17. Modeled El Pilar fault-generated tsunami effects at Malmok beach (Aruba). a) Flooding map at Malmok beach obtained using the Celeris software (DEM derived from TanDEM X). b) Coral debris within cactus plants observed in Malmok lagoon.

boulders being displaced multiple times due to different tsunami events have been studied in Australia; in these cases, top-cliff boulders weighing 20–100 tons were moved up to 100 m inland by two Holocene tsunami events (Scheffers et al., 2008). In this study, the location of the coastal boulders of the ABC Islands may be the culmination of different tsunami events that drove boulder transport as indicated by the paleo-landscape reconstruction of the 500 years BP scenario.

5.3. Inundation surfaces and boulder accumulations

The impact of tsunamis and storm waves can result in the severe inundation of the three studied islands. Pignatelli et al. (2010) showed that the inundation limit was located further inland than the positions of the tsunami-transported boulders. Using paleo-landscape reconstructions at Tierra del Sol on Aruba, which was hit by relatively small waves compared to Bonaire and Curaçao (Fig. 14), we simulated the paleo-landscape inundation caused by the impact of tsunamis that occurred 500 and 4000 years BP and compared them to the flooding caused by Hurricane Ivan (September 2004) under present sea-level conditions (Fig. 15a). In general, the inundation extent was similar for all events, extending a maximum of 200 m inland. This similarity between these events makes determining the scenario responsible for the observed boulder displacement more challenging. For example, the impact of hurricanes has occasionally led to the displacement of some boulders, such as was observed during Hurricane Ivan in Bonaire (Scheffers and Scheffers, 2006; Engel and May 2012).

Small boulders were observed to be sorted along the ridge deposits, with their a-axis values decreasing in length landward (Fig. 16). The presence of ridge deposits resulting from hurricane impacts on the ABC Islands has been discussed in previous studies (Morton et al., 2008; Spiske et al., 2008). Nevertheless, there are boulders weighing over 50 tons that have not been displaced by hurricanes (Scheffers and Scheffers,

2006; Engel and May 2012). Some coral debris and overwash deposits were observed in the back lagoon located at Malmok Beach (Aruba; Fig. 17). This may be related to the El Pilar earthquake-generated tsunami, which produced water levels of ~3 m, resulting in a maximum inundation surface that extended across the lagoon. A similar pattern was observed in Salina Tam (leeward Bonaire; Engel et al., 2012b), where high-energy deposits were observed in sedimentary cores and attributed to episodic tsunami events.

6. Conclusions

The coastal boulders of the ABC islands represent out-of-size deposits that may be related to tsunami or storm events. The dimensional features and distributions of these deposits are important factors that can be used to constrain the type of event that was responsible for their displacement. Here, SfM/MVS methods allowed us to obtain high-resolution dimensional data of the studied coastal boulders as well as reconstruct paleo-landscapes in the ABC islands. Radiocarbon dating allowed for the identification of three key event horizons associated with multiple extreme wave occurrences: 500, 2000, and 4000 years BP. Given the distance of the boulders from the surf zone (more than 100 m in some cases), these displacements are likely to have occurred at different times. The onset of boulder displacement is most likely to be associated with the oldest key horizon (4000 years BP), corresponding to a sea-level position of −1.65 m and a paleo shoreline located about 60 m seaward. An analysis of the incipient motion of the boulders combined with numerical models and chronological constraints revealed that the events responsible for boulder displacement would have resulted in high flow velocities in Bonaire and slightly lower velocities in Curaçao and Aruba. The overall displacement of the coastal boulders is likely to have been caused by multiple events across the three key event horizons.

Based on hydrodynamic simulations and the calculated wave flow velocities required to move the boulders, the most likely tsunamigenic scenario is associated with slip along the El Pilar fault system (a Venezuelan structure); this hypothesis is supported by water level models of tsunami propagation. Furthermore, the cross-shore velocities of the modeled El Pilar fault-generated tsunami resulted in higher values than the required flows as indicated by incipient motion formulas. The El Pilar fault-generated tsunami models were also consistent with other geomorphological evidence of coastal flooding detected in Aruba. While hurricanes can result in the deposition of imbricated ridges and may have influenced the current positions of the coastal boulders across the islands, we show that the initial and main factors that drive coastal boulder transport are likely related to the impacts of different tsunamis across multiple event horizons.

Author contributions

Conceptualization: Giovanni Scardino, Giovanni Scicchitano; Data Curation: Giovanni Scardino, Denovan Chauveau, Patrick Boyden, Alessio Rovere; Formal analysis: Giovanni Scicchitano, Alessio Rovere, N.A.K. Nandasena; Funding acquisition: Giovanni Scicchitano, Alessio Rovere, Giovanni Scardino, Patrick Boyden; Investigation: Giovanni Scardino, Malena Dahm, Sonia Bejarano, Giovanni Scicchitano, Alessio Rovere, Eric Mijts, Harold Kelly. Methodology: Giovanni Scardino, N.A.K. Nandasena, Elisa Casella, Alessio Rovere, Patrick Boyden, Denovan Chauveau, Chiara Barile. Project administration: Alessio Rovere, Patrick Boyden, Giovanni Scicchitano. Resources: Alessio Rovere, Patrick Boyden, Giovanni Scicchitano, Giovanni Scardino. Software: Giovanni Scardino, Chiara Barile, Alessio Rovere. Supervision: Alessio Rovere, Giovanni Scicchitano, Eric Mijts, Harold Kelly. Validation: Alessio Rovere, Elisa Casella, Patrick Boyden, Denovan Chauveau. Visualization: Eric Mijts, Harold Kelly, Sonia Bejarano. Roles/Writing - original draft: Giovanni Scardino, Giovanni Scicchitano and Writing - review & editing: Alessio Rovere, Patrick Boyden, Denovan Chauveau.

Funding

This work was developed as part of the activities of the Research Agreement stipulated between the University of Bari Aldo Moro and the Agenzia Regionale Strategica per lo Sviluppo Ecosostenibile del Territorio (ASSET, Italy) (Scientific Coordinator Giovanni Scicchitano).

PB (Patrick Boyden), AR (Alessio Rovere), SB (Sonia Bejarano), and MD (Malena Dahm) were funded by the Deutsche Forschungsgemeinschaft (DFG, German Research Foundation) – Project number 468589501 – SPP 2299/Project number 441832482.

Declaration of competing interest

The authors declare that they have no known competing financial interests or personal relationships that could have appeared to influence the work reported in this paper.

Acknowledgments

We acknowledge the ERC SEED UNIBA project “Get aHead Of the MEdicanes: strategies for the COASTal environment—HOME-COAST” (Principal Investigator Giovanni Scardino, PhD). We would also like to thank the Washington Slagbaai National Park (Bonaire) and Arikok National Park (Aruba). We are thankful to the reviewers that allowed us to improve this work. An initial version of this work was developed by Chiara Barile in the framework of her master thesis at the University of Bari-Department of Geoenvironmental Sciences.

Appendix A. Supplementary data

Supplementary data to this article can be found online at https://doi.org/10.1016/j.quascirev.2024.109136.

Data availability

Data will be made available on request.

References

Alexander, C., 1961. The marine terraces of Aruba, Bonaire, and Curacao, Netherlands Antilles. Ann. Assoc. Am. Geogr. 51, 102–123. https://doi.org/10.1111/j.1467-8306.1961.tb00370.x.

Audemard, F.A., 2007. Revised seismic history of the El Pilar fault, Northeastern Venezuela, from the Cariaco 1997 earthquake and recent preliminary paleoseismic results. J. Seismol. 11, 311–326. https://doi.org/10.1007/s10950-007-9054-2.

Avé Lallemant, H.G., 1997. Transpression, displacement partitioning, and exhumation in the eastern Caribbean/South American plate boundary zone. Tectonics 16, 272–289. https://doi.org/10.1029/96TC03725.

Baptista, M., Heitor, S., Miranda, J., Miranda, P., Victor, L., 1998. The 1755 Lisbon tsunami; Evaluation of the tsunami parameters. J. Geodynam. 25, 143–157. https://doi.org/10.1016/S0264-3707(97)00019-7.

Beardsley, A.G., Avé Lallemant, H.G., 2007. Oblique collision and accretion of The Netherlands Leeward Antilles to South America. Tectonics 26. https://doi.org/10.1029/2006TC002028.

Boudon, G., Semet, M., Vincent, P., 1984. Flank failure–directed blast eruption at Soufrière, Guadeloupe, French West Indies: a 3,000-yr-old Mt. St. Helens? Geology 12. https://doi.org/10.1130/0091-7613(1984)12<350:FFBEAS>2.0.CO;2.

Bernard, P., Lambert, J., 1988. Subduction and seismic hazard in the northern Lesser Antilles: Revision of the historical seismicity. Bulletin of the Seismological Society of America 78, 1965–1983. https://doi.org/10.1785/BSSA0780061965.

Boudon, G., Le Friant, A., Komorowski, J.-C., Deplus, C., Semet, M.P., 2007. Volcano flank instability in the Lesser Antilles Arc: diversity of scale, processes, and temporal recurrence. J. Geophys. Res. Solid Earth 112. https://doi.org/10.1029/2006JB004674.

Boudon, G., Semet, M., Vincent, P., 1984. Flank failure–directed blast eruption at Soufrière, Guadeloupe, French West Indies: A 3,000-yr-old Mt. St. Helens? Geology 12. https://doi.org/10.1130/0091-7613.

Bries, J.M., Debrot, A.O., Meyer, D.L., 2004. Damage to the leeward reefs of Curaçao and Bonaire, Netherlands Antilles from a rare storm event: hurricane Lenny, November 1999. Coral Reefs 23, 297–307. https://doi.org/10.1007/s00338-004-0379-9.

ten Brink, U., Twichell, D., Geist, E., Chaytor, J., Locat, J., Lee, H., Buczkowski, B., Barkan, R., Solow, A.R., Andrews, B., Parsons, T., Lynett, P., Lin, J., Sansoucy, M., 2008. Evaluation of Tsunami Sources with the Potential to Impact the U.S. Atlantic

and Gulf Coasts: An Updated Report to the Nuclear Regulatory Commission.Nuclear Regulatory Commission 1, 1–322.
Brink, U. ten, Wei, Y., Fan, W., Granja Bruña, J.-L., Miller, N., 2020. Mysterious tsunami in the Caribbean Sea following the 2010 Haiti earthquake possibly generated by dynamically triggered early aftershocks. Earth Planet Sci. Lett. 540, 116269. https://doi.org/10.1016/j.epsl.2020.116269.
Calais, E., Perrot, J., Lépinay, B.M. de, 1998. Strike-slip tectonics and seismicity along the northern Caribbean plate boundary from Cuba to Hispaniola. In: Dolan, J.F., Mann, P. (Eds.), Active Strike-Slip and Collisional Tectonics of the Northern Caribbean Plate Boundary Zone. Geological Society of America. https://doi.org/10.1130/0-8137-2326-4.125.
Colón, S., Audemard, F.A., Beck, C., Avila, J., Padrón, C., De Batist, M., Paolini, M., Leal, A.F., Van Welden, A., 2015. The 1900 Mw 7.6 earthquake offshore north–central Venezuela: Is La Tortuga or San Sebastián the source fault? Marine and Petroleum Geology 67, 498–511. https://doi.org/10.1016/j.marpetgeo.2015.06.005.
Costa, P.J.M., Dawson, S., Ramalho, R.S., Engel, M., Dourado, F., Bosnic, I., Andrade, C., 2021. A review on onshore tsunami deposits along the Atlantic coasts. Earth Sci. Rev. 212, 103441. https://doi.org/10.1016/j.earscirev.2020.103441.
Cox, R., Ardhuin, F., Dias, F., Autret, R., Beisiegel, N., Earlie, C.S., Herterich, J.G., Kennedy, A., Paris, R., Raby, A., Schmitt, P., Weiss, R., 2020. Systematic review shows that work done by storm waves can Be misinterpreted as tsunami-related because commonly used hydrodynamic equations are flawed. Front. Mar. Sci. 7. https://doi.org/10.3389/fmars.2020.00004.
Cox, R., Jahn, K.L., Watkins, O.G., Cox, P., 2018. Extraordinary boulder transport by storm waves (west of Ireland, winter 2013–2014), and criteria for analysing coastal boulder deposits. Earth-Science Reviews 177, 623–636. https://doi.org/10.1016/j.earscirev.2017.12.014.
de Lange, W.P., de Lange, P.J., Moon, V.G., 2006. Boulder transport by waterspouts: An example from Aorangi Island, New Zealand. Marine Geology 230, 115–125. https://doi.org/10.1016/j.margeo.2006.04.006.
Delle Rose, M., 2024. Annual coastal boulder mobility detected in 2017–2021 remote sensing imagery and its relation to marine storms (Gulf of Taranto, Mediterranean Sea). Geosciences 14, 136. https://doi.org/10.3390/geosciences14050136.
Delle Rose, M., Fidelibus, C., Martano, P., Orlanducci, L., 2020. Storm-induced boulder displacements: inferences from field surveys and hydrodynamic equations. Geosciences 10, 1–21. https://doi.org/10.3390/geosciences10090374.
Dewey, J.F., Goff, J., Ryan, P.D., 2021. The origins of marine and non-marine boulder deposits: a brief review. Nat. Hazards 109, 1981–2002. https://doi.org/10.1007/s11069-021-04906-3.
DiNapoli, R.J., Fitzpatrick, S.M., Napolitano, M.F., Rick, T.C., Stone, J.H., Jew, N.P., 2021. Marine reservoir corrections for the Caribbean demonstrate high intra- and inter-island variability in local reservoir offsets. Quat. Geochronol. 61, 101126. https://doi.org/10.1016/j.quageo.2020.101126.
Dondin, F., Jean-Frédéric, L., Kelfoun, K., Fournier, N., Randrianasolo, A., 2012. Sector collapse at Kick 'em Jenny submarine volcano (Lesser Antilles): numerical simulation and landslide behaviour. Bull. Volcanol. 74, 595–607. https://doi.org/10.1007/s00445-011-0554-0.
Dunán-Avila, P., Authemayou, C., Jaud, M., Pedoja, K., Jara-Muñoz, J., Bertín, S., Peñalver-Hernández, L., Floc'h, F., Nuñez-Labañino, A., Winckler, P., Pierre-Toledo, J., Jesus Benítez-Frometa, P. de, Ross-Cabrera, H., Letortu, P., Rodríguez-Valdés, A.R., Coutín-Lobaina, N., Chauveau, D., 2024. Geomorphological signatures of known hurricanes and validation of theoretical emplacement formulations: coastal boulder deposits on Cuban low-lying marine terraces. Mar. Geol. 107438. https://doi.org/10.1016/j.margeo.2024.107438.
Dutch Caribbean Biodiversity Database [WWW Document], 2019. URL. https://www.dcbd.nl/resource/2319, 7.22.24.
Engel, M., Brückner, H., Wennrich, V., Scheffers, A., Kelletat, D., Vött, A., Schäbitz, F., Daut, G., Willershäuser, T., May, S.M., 2010. Coastal stratigraphies of eastern Bonaire (Netherlands Antilles): New insights into the palaeo-tsunami history of the southern Caribbean. Sedimentary Geology 231, 14.
Engel, M., May, S.M., 2012. Bonaire's boulder fields revisited: evidence for Holocene tsunami impact on the Leeward Antilles. Quat. Sci. Rev. 54, 126–141, 10.1016/j.quascirev.2011.12.011.
Engel, M., Brückner, H., Fürstenberg, S., Frenzel, P., Irrgang, A., Scheffers, A., Kelletat, D., May, S., Schäbitz, F., Daut, G., 2012a. A prehistoric tsunami induced long-lasting ecosystem changes on a semi-arid tropical island - the case of Boka Bartol (Bonaire, Leeward Antilles). Naturwissenschaften 100. https://doi.org/10.1007/s00114-012-0993-2.
Engel, M., Brückner, H., Messenzehl, K., Frenzel, P., May, S.M., Scheffers, A., Scheffers, S., Wennrich, V., Kelletat, D., 2012b. Shoreline changes and high-energy wave impacts at the leeward coast of Bonaire (Netherlands Antilles). Earth Planets Space 64, 9. https://doi.org/10.5047/eps.2011.08.011.
Engel, M., Brückner, H., Scheffers, S., May, S., Kelletat, D., 2014. Holocene sea levels of Bonaire (Leeward Antilles) and tectonic implications. Zeitschrift für Geomorphologie Supplementary Issues 58, 159–178. https://doi.org/10.1127/0372-8854/2012/S-00111.
Evelpidou, N., Zerefos, C., Synolakis, C., Repapis, C., Karkani, A., Polidorou, M., Saitis, G., 2020. Coastal boulders on the SE coasts of Cyprus as evidence of palaeo-tsunami events. J. Mar. Sci. Eng. 8, 812. https://doi.org/10.3390/jmse8100812.
Focke, J.W., 1978. Limestone cliff morphology and organism distribution on Curaçao (Netherlands Antilles). Leidse Geol. Meded. 51, 131–150.
Fouke, B., Beets, C., Meyers, W., Hanson, G., Melillo, A., 1996. Sr-87/Sr-86 chronostratigraphy and dolomitization history of the Seroe Domi formation, Curacao (Netherlands Antilles). Facies 35, 293–320.
French, C.D., Schenk, C.J., 2004. Map Showing Geology, Oil and Gas Fields, and Geologic Provinces of the Caribbean Region. U.S. Geological Survey. https://doi.org/10.3133/ofr97470K. No. 97-470- K), Open-File Report.
Fritz, H., Hillaire, J., Molière, E., Wei, Y., Mohammed, F., 2013. Twin tsunamis triggered by the 12 January 2010 Haiti earthquake. Pure Appl. Geophys. 170, 1463–1474. https://doi.org/10.1007/s00024-012-0479-3.
Gianfreda, F., Mastronuzzi, G., Sansò, P., 2001. Impact of historical tsunamis on a sandy coastal barrier: an example from the northern Gargano coast, southern Italy. Nat. Hazards Earth Syst. Sci. 1, 213–219. https://doi.org/10.5194/nhess-1-213-2001.
Goto, K., Okada, K., Imamura, F., 2009. Characteristics and hydrodynamics of boulders transported by storm waves at Kudaka Island, Japan. Mar. Geol. 262, 14–24. https://doi.org/10.1016/j.margeo.2009.03.001.
Goto, K., Miyagi, K., Kawamata, H., Imamura, F., 2010. Discrimination of boulders deposited by tsunamis and storm waves at Ishigaki Island, Japan. Mar. Geol. 269, 34–45. https://doi.org/10.1016/j.margeo.2009.12.004.
Goto, K., Miyagi, K., Kawana, T., Takahashi, J., Imamura, F., 2011. Emplacement and movement of boulders by known storm waves — field evidence from the Okinawa Islands, Japan. Marine Geology, Special Issue on Boulders as a signature of storms on rock coasts 283, 66–78. https://doi.org/10.1016/j.margeo.2010.09.007.
Harbitz, C., Løvholt, F., Pedersen, G., Masson, D., 2006. Mechanisms of tsunami generation by submarine landslides: a short review. Nor. Geol. Tidsskr. 86, 255–264.
Hall, A.M., 2011. Storm wave currents, boulder movement and shore platform development: A case study from East Lothian, Scotland. Marine Geology, Special Issue on Boulders as a signature of storms. on rock coasts 283, 98–105. https://doi.org/10.1016/j.margeo.2010.10.024.
Hall, A., Hansom, J., Williams, D., Jarvis, J., 2006. Distribution, geomorphology and lithofacies of cliff-top storm deposits: Examples from the high-energy coasts of Scotland and Ireland. Marine Geology 232, 131–155. https://doi.org/10.1016/j.margeo.2006.06.008.
Harbitz, C.B., Glimsdal, S., Bazin, S., Zamora, N., Løvholt, F., Bungum, H., Smebye, H., Gauer, P., Kjekstad, O., 2012. Tsunami hazard in the Caribbean: Regional exposure derived from credible worst case scenarios. Continental Shelf Research 38, 1–23. https://doi.org/10.1016/j.csr.2012.02.006.
Harbitz, C.B., Løvholt, F., Bungum, H., 2014. Submarine landslide tsunamis: how extreme and how likely? Nat. Hazards 72, 1341–1374. https://doi.org/10.1007/s11069-013-0681-3.
Hoeksema, B., Harper, C., Langdon-Down, S., van der Schoot, R., Smith-Moorhouse, A., Spaargaren, R., Timmerman, R., 2022. Host range of the coral-associated worm Snail Petaloconchus sp. (Gastropoda: Vermetidae), a newly discovered cryptogenic pest species in the southern Caribbean. Diversity 14, 196. https://doi.org/10.3390/d14030196.
Jouanne, F., Audemard, F.A., Beck, C., Van Welden, A., Ollarves, R., Reinoza, C., 2011. Present-day deformation along the El Pilar Fault in eastern Venezuela: evidence of creep along a major transform boundary. J. Geodyn. 51, 398–410. https://doi.org/10.1016/j.jog.2010.11.003.
Khan, N.S., Ashe, E., Horton, B.P., Dutton, A., Kopp, R.E., Brocard, G., Engelhart, S.E., Hill, D.F., Peltier, W.R., Vane, C.H., Scatena, F.N., 2017. Drivers of Holocene sea-level change in the Caribbean. Quat. Sci. Rev. 155, 13–36. https://doi.org/10.1016/j.quascirev.2016.08.032.
Klosowska, B.B., 2003. Late Holocene Embayment and Salina Record of Curacao (Dutch Antilles): Criteria to Monitor Environmental Cnage and Biodiversity (PhD-Thesis - Research and Graduation Internal). VU, Amsterdam.
Lander, J., LowellS, W., Lockridge, P., 2002. A brief history of tsunami in the Caribbean Sea. Sci. Tsunami Hazards 20.
Lario, J., Spencer, C., Bardají, T., Marchante, Á., Garduño-monroy, V.H., Macias, J., Ortega, S., 2020. An extreme wave event in eastern Yucatán, Mexico: evidence of a palaeotsunami event during the Mayan times. Sedimentology 67, 1481–1504. https://doi.org/10.1111/sed.12662.
Lario, J., Spencer, C., Bardají, T., 2023. Presence of boulders associated with an extreme wave event in the western Mediterranean (Cape Cope, Murcia, Spain): possible evidence of a tsunami. J. Iber. Geol. 49, 115–132. https://doi.org/10.1007/s41513-023-00208-8.
Le Friant, A., Boudon, G., Deplus, C., Villemant, B., 2003. Large-scale flank collapse events during the activity of Montagne Pelée, Martinique, Lesser Antilles. J. Geophys. Res. Solid Earth 108. https://doi.org/10.1029/2001JB001624.
Le Quéré, P.A., Nistor, I., Mohammadian, A., 2020. Numerical modeling of tsunami-induced scouring around a square column: performance assessment of FLOW-3D and Delft3D. J. Coast Res. 36, 1278–1291. https://doi.org/10.2112/JCOASTRES-D-19-00181.1.
Leslie, S.C., Mann, P., 2016. Giant submarine landslides on the Colombian margin and tsunami risk in the Caribbean Sea. Earth Planet Sci. Lett. 449, 382–394. https://doi.org/10.1016/j.epsl.2016.05.040.
Lindsay, J., Shepherd, J., Wilson, D., 2005. Volcanic and scientific activity at kick 'em Jenny submarine volcano 2001–2002: implications for volcanic hazard in the southern Grenadines, Lesser Antilles. Nat. Hazards 34, 1–24. https://doi.org/10.1007/s11069-004-1566-2.
Lorscheid, T., Stocchi, P., Casella, E., Gómez-Pujol, L., Vacchi, M., Mann, T., Rovere, A., 2017. Paleo sea-level changes and relative sea-level indicators: precise measurements, indicative meaning and glacial isostatic adjustment perspectives from Mallorca (Western Mediterranean). Palaeogeogr. Palaeoclimatol. Palaeoecol. 473, 94–107. https://doi.org/10.1016/j.palaeo.2017.02.028.
Mastronuzzi, G., Sansò, P., 2000. Boulders transport by catastrophic waves along the Ionian coast of Apulia (southern Italy). Mar. Geol. 170, 93–103. https://doi.org/10.1016/S0025-3227(00)00068-2.
Mattioli, 1995. ABSTRACT: Flank Failure or Caldera Collapse on an Island Arc Volcano? A Digital Elevation Study of the Qualibou Depression. St. Lucia.

May, S.M., Vött, A., Brückner, H., Smedile, A., 2012. The Gyra washover fan in the Lefkada Lagoon, NW Greece—possible evidence of the 365 AD Crete earthquake and tsunami. Earth Planets Space 64, 859–874. https://doi.org/10.5047/eps.2012.03.007.
Morton, R., Richmond, B., Jaffe, B., Gelfenbaum, G., 2006. Reconnaissance investigation of Caribbean extreme wave deposits - preliminary observations, interpretations, and research directions. Open-File Report 2006-1293.
Morton, R.A., Richmond, B.M., Jaffe, B.E., Gelfenbaum, G., 2008. Coarse-clast ridge complexes of the Caribbean: a preliminary basis for distinguishing tsunami and storm-wave origins. J. Sediment. Res. https://doi.org/10.2110/jsr.2008.068.
Muhs, D.R., Pandolfi, J.M., Simmons, K.R., Schumann, R.R., 2012. Sea-level history of past interglacial periods from uranium-series dating of corals, Curaçao, Leeward Antilles islands. Quaternary Research 78, 157–169. https://doi.org/10.1016/j.yqres.2012.05.008.
Nandasena, N.A.K., Paris, R., Tanaka, N., 2011a. Numerical assessment of boulder transport by the 2004 Indian Ocean Tsunami in Lhok Nga, west Banda Aceh (Sumatra, Indonesia). Comput. Geosci. 37, 1391–1399. https://doi.org/10.1016/j.cageo.2011.02.001.
Nandasena, N.A.K., Paris, R., Tanaka, N., 2011b. Reassessment of hydrodynamic equations: minimum flow velocity to initiate boulder transport by high energy events (storms, tsunamis). Mar. Geol. 281, 70–84. https://doi.org/10.1016/j.margeo.2011.02.005.
Nandasena, N.A.K., Tanaka, N., Sasaki, Y., Osada, M., 2013. Boulder transport by the 2011 Great East Japan tsunami: comprehensive field observations and whither model predictions? Mar. Geol. 346, 292–309. https://doi.org/10.1016/j.margeo.2013.09.015.
Nandasena, N.A.K., Scicchitano, G., Scardino, G., Milella, M., Piscitelli, A., Mastronuzzi, G., 2022. Boulder displacements along rocky coasts: a new deterministic and theoretical approach to improve incipient motion formulas. Geomorphology 407, 108217. https://doi.org/10.1016/j.geomorph.2022.108217.
NGDC, N.G.D., 2021. Global Historical Tsunami Database | NCEI [WWW Document]. Global Historical Tsunami Database | NCEI - doi:10.7289/V5PN93H7. URL. https://www.ngdc.noaa.gov/hazard/tsu_db.shtml, 4.9.24.
NHC-NOAA, 2024. Tropical Cyclone Climatology [WWW Document]. URL. https://www.nhc.noaa.gov/climo/#hrhm, 9.2.24.
Nott, J., 2003a. Tsunami or storm waves?:determining the origin of a spectacular field of wave emplaced boulders using numerical storm surge and wave models and hydrodynamic transport equations. J. Coast Res. 19, 348–356.
Nott, J., 2003b. Waves, coastal boulder deposits and the importance of the pre-transport setting. Earth Planet Sci. Lett. 210, 269–276. https://doi.org/10.1016/S0012-821X(03)00104-3.
Obert, J., Scholz, D., Felis, T., Brocas, W., Jochum, K., Andreae, M., 2016. 230Th/U dating of Last Interglacial brain corals from Bonaire (southern Caribbean) using bulk and theca wall material. Geochem. Cosmochim. Acta 178, 20–40. https://doi.org/10.1016/j.gca.2016.01.011.
Oetjen, J., Engel, M., Effkemann, C., 2015. Numerical modelling of tsunami scenarios for the island of Bonaire (Leeward Antilles).
Oetjen, J., Engel, M., Pudasaini, S.P., Schuettrumpf, H., 2020. Significance of boulder shape, shoreline configuration and pre-transport setting for the transport of boulders by tsunamis. Earth Surf. Process. Landforms 45, 2118–2133. https://doi.org/10.1002/esp.4870.
O'Loughlin, K.F., Lander, J.F., 2003. Caribbean Tsunamis: A 500-Year History from 1498-1998, 1. Springer Science & Business Media, pp. 1–286.
Pararas-Carayannis, G., 2010. Assessment of the tsunamigenic potential along the northern Caribbean margin - case study: earthquake and tsunamis of 12 January 2010 in Haiti. Sci. Tsunami Hazards 29.
Paris, R., Fournier, J., Poizot, E., Etienne, S., Morin, J., Lavigne, F., Wassmer, P., 2010. Boulder and fine sediment transport and deposition by the 2004 tsunami in Lhok Nga (western Banda Aceh, Sumatra, Indonesia): a coupled offshore–onshore model. Mar. Geol. 268, 43–54. https://doi.org/10.1016/j.margeo.2009.10.011.
Pavlis, N.K., Holmes, S.A., Kenyon, S.C., Factor, J.K., 2012. The development and evaluation of the Earth gravitational model 2008 (EGM2008). J. Geophys. Res. Solid Earth 117. https://doi.org/10.1029/2011JB008916.
Pedoja, K., Dunán-Avila, P., Jara-Muñoz, J., Authemayou, C., Nuñez-Labañino, A., Gelder, G. de, Chauveau, D., Peñalver, L., Frometa, P.D.J.B., Martin-Izquierdo, D., Abella, E.C., Bertin, S., Rodríguez-Valdés, Á.R., Arango-Arias, E.D., Traoré, K., Regard, V., 2023. On a 210 t Caribbean coastal boulder: the huracanolito seaward of the ruins of the Bucanero resort, Juragua, Oriente, Cuba. Earth Surf. Process. Landforms 48, 3074–3090. https://doi.org/10.1002/esp.5682.
Perez, O., Wesnousky, S., De La Rosa, R., Márquez, J., Uzcategui, R., Quintero, C., Liberal, L., Mora-Paez, H., Szeliga, W., 2018. On the interaction of the North Andes plate with the Caribbean and South American plates in northwestern South America from GPS geodesy and seismic data. Geophys. J. Int. 214, 1986–2001. https://doi.org/10.1093/gji/ggy230.
Pignatelli, C., Sansò, P., Mastronuzzi, G., 2009. Evaluation of tsunami flooding using geomorphologic evidence. Marine Geology 260, 6–18. https://doi.org/10.1016/j.margeo.2009.01.002.
Pignatelli, C., Scheffers, A., Scheffers, S., Mastronuzzi, G., 2010. Assessment of extreme wave flooding from geomorphologic evidence in Bonaire (Netherlands antilles). Zeitschrift fur Geomorphologie 54, 219–245. https://doi.org/10.1127/0372-8854/2010/0054S3-0026.
Pollyea, R.M., Fairley, J.P., 2012. Experimental evaluation of terrestrial LiDAR-based surface roughness estimates. Geosphere 8, 222–228. https://doi.org/10.1130/GES00733.1.
Poupardin, A., Calais, E., Heinrich, P., Hébert, H., Rodriguez, M., Leroy, S., Aochi, H., Douilly, R., 2020. Deep submarine landslide contribution to the 2010 Haiti earthquake tsunami. Nat. Hazards Earth Syst. Sci. 20, 2055–2065. https://doi.org/10.5194/nhess-20-2055-2020.
Pousse Beltran, L., Pathier, E., Jouanne, F., Vassallo, R., Reinoza, C., Audemard, F., Doin, M., Volat, M., 2016. Spatial and temporal variations in creep rate along the El Pilar fault at the Caribbean-South American plate boundary (Venezuela), from InSAR.: Aseismic slip along the El Pilar fault. Journal of Geophysical Research: Solid Earth 121. https://doi.org/10.1002/2016JB013121.
Radtke, U., Schellmann, G., Scheffers, A., Kelletat, D., Kromer, B., Kasper, H., 2003. Electron spin resonance and radiocarbon dating of coral deposited by Holocene tsunami events on Curacao, Bonaire and Aruba (Netherlands Antilles). School of Environmental Science and Management Papers 22. https://doi.org/10.1016/S0277-3791(03)00036-2.
Rixhon, G., May, S.M., Engel, M., Mechernich, S., Schroeder-Ritzrau, A., Frank, N., Fohlmeister, J., Boulvain, F., Dunai, T., Brückner, H., 2018. Multiple dating approach (14C, 230Th/U and 36Cl) of tsunami-transported reef-top boulders on Bonaire (Leeward Antilles) – current achievements and challenges. Mar. Geol., Geol. Records Extreme Wave Events 396, 100–113. https://doi.org/10.1016/j.margeo.2017.03.007.
Robinson, E., Rowe, D.-A.C., Khan, S.A., 2006. Wave-emplaced boulders on Jamaica's rocky shores. Z. Geomorphol., Suppl. 146, 39–57.
Roig-Munar, F.X., Gelabert, B., Rodríguez-Perea, A., Martín-Prieto, J.Á., Vilaplana, J.M., 2023. Storm or tsunamis: boulder deposits on the rocky coasts of the Balearic Islands (Spain). Mar. Geol. 463, 107112. https://doi.org/10.1016/j.margeo.2023.107112.
Rovere, A., Casella, E., Harris, D.L., Lorscheid, T., Nandasena, N.A.K., Dyer, B., Sandstrom, M.R., Stocchi, P., D'Andrea, W.J., Raymo, M.E., 2017. Giant boulders and Last Interglacial storm intensity in the North Atlantic. Proceedings of the National Academy of Sciences of the United States of America 114, 12144–12149. https://doi.org/10.1073/pnas.1712433114.
Roy, K., Peltier, W.R., 2015. Glacial isostatic adjustment, relative sea level history and mantle viscosity: reconciling relative sea level model predictions for the U.S. East coast with geological constraints. Geophys. J. Int. 201, 1156–1181. https://doi.org/10.1093/gji/ggv066.
Roy, K., Peltier, W.R., 2017. Space-geodetic and water level gauge constraints on continental uplift and tilting over North America: regional convergence of the ICE-6G_C (VM5a/VM6) models. Geophys. J. Int. 210, 1115–1142. https://doi.org/10.1093/gji/ggx156.
Roy, K., Peltier, W.R., 2018. Relative sea level in the Western Mediterranean basin: a regional test of the ICE-7G_NA (VM7) model and a constraint on late Holocene Antarctic deglaciation. Quat. Sci. Rev. 183, 76–87. https://doi.org/10.1016/j.quascirev.2017.12.021.
Scardino, G., Piscitelli, A., Milella, M., Sansò, P., Mastronuzzi, G., 2020. Tsunami fingerprints along the Mediterranean coasts. Rendiconti Lincei. Sci. Fis. Nat. 31, 319–335. https://doi.org/10.1007/s12210-020-00895-w.
Scheffers, A., 2002. Paleotsunami evidences from boulder deposits on Aruba. Curaçao Bonaire.
Scheffers, A., 2004. Tsunami imprints on the Leeward Netherlands Antilles (Aruba, Curaçao, Bonaire) and their relation to other coastal problems. Quaternary international, coastal environmental change during sea-level highstands. IGCP 437 Symposium, Barbados 120, 163–172. https://doi.org/10.1016/j.quaint.2004.01.015.
Scheffers, A., 2005. Coastal response to extreme wave events: hurricanes and tsunami on Bonaire. Anja Scheffers.
Scheffers, A., Kelletat, D., 2006. New evidence and datings of holocene paleo-tsunami events in the caribbean (Barbados, st. martin and Anguilla). In: Caribbean Tsunami Hazard. WORLD SCIENTIFIC, pp. 178–202. https://doi.org/10.1142/9789812774613_0008.
Scheffers, A., Scheffers, S., 2006. Documentation of the impact of hurricane Ivan on the coastline of Bonaire (Netherlands Antilles). J. Coast Res. 22, 1437–1452.
Scheffers, A., Engel, M., Scheffers, S., May, S.M., Hänßler, E., Löhr, K., Joannes-Boyau, R., Kelletat, D., Brückner, H., Vött, A., Schellmann, G., Schäbitz, F., Radtke, U., Sommer, B., 2014. Coastal landforms and event histories in a tropical carbonate environment. In: Martini, I.P. (Ed.), Coastal Environments: from the Arctic to the Tropics, vol. 388, pp. 503–531. Geol. Soc. Lond. Spec. Publ.
Scheffers, S., Scheffers, A., Kelletat, D., Bryant, E., 2008. The Holocene paleo-tsunami history of West Australia. School of Environmental Science and Management Papers 270. https://doi.org/10.1016/j.epsl.2008.03.027.
Scheffers, S.R., Haviser, J., Browne, T., Scheffers, A., 2009. Tsunamis, hurricanes, the demise of coral reefs and shifts in prehistoric human populations in the Caribbean. Quaternary International, Hurricanes and Typhoons: From the Field Records to the Forecast 195, 69–87. https://doi.org/10.1016/j.quaint.2008.07.016.
Schubert, C., 1994. Tsunamis in Venezuela: Some Observations on their Occurrence. Journal of Coastal Research 189–195.
Scicchitano, G., Monaco, C., Tortorici, L., 2007. Large boulder deposits by tsunami waves along the Ionian coast of south-eastern Sicily (Italy). Marine Geology 238, 75–91. https://doi.org/10.1016/j.margeo.2006.12.005.
Scicchitano, G., Pignatelli, C., Spampinato, C.R., Piscitelli, A., Milella, M., Monaco, C., Mastronuzzi, G., 2012. Terrestrial Laser Scanner techniques in the assessment of tsunami impact on the Maddalena peninsula (south-eastern Sicily, Italy). Earth, Planets and Space 64, 889–903. https://doi.org/10.5047/eps.2011.11.009.
Scicchitano, G., Scardino, G., Tarascio, S., Monaco, C., Barracane, G., Locuratolo, G., Milella, M., Piscitelli, A., Mazza, G., Mastronuzzi, G., 2020. The first video witness of coastal boulder displacements recorded during the impact of Medicane. "Zorbas" on Southeastern Sicily. Water 12, 1497. https://doi.org/10.3390/w12051497.
Smith, M.S., Shepherd, J.B., 1993a. Explosive submarine eruptions of kick-'Em-Jenny volcano : preliminary investigations of the potential tsunami hazard in the Eastern

Caribbean region. In: Proccedings of the Caribbean Conference on Natural Hazards : Volcanoes, Earthquakes, Windstorms, Floods, pp. 249–260.
Smith, M.S., Shepherd, J.B., 1993b. Preliminary investigations of the tsunami hazard of Kick'em Jenny submarine volcano. Nat. Hazards 7, 257–277. https://doi.org/10.1007/BF00662650.
Spiske, M., Böröcz, Z., Bahlburg, H., 2008. The role of porosity in discriminating between tsunami and hurricane emplacement of boulders — a case study from the Lesser Antilles, southern Caribbean. Earth Planet Sci. Lett. 268, 384–396. https://doi.org/10.1016/j.epsl.2008.01.030.
Stuiver, M., Reimer, P.J., 1993. Extended 14C data base and revised CALIB 3.0 14C age Calibration program. Radiocarbon 35, 215–230. https://doi.org/10.1017/S0033822200013904.
Stuiver, M., Reimer, P.J., Reimer, R.W., 2021. CALIB 14C Calibration Program [WWW Document]. URL. http://calib.org/calib/, 7.27.21.
Tavakkol, S., Lynett, P., 2017. Celeris: a GPU-accelerated open source software with a Boussinesq-type wave solver for real-time interactive simulation and visualization. Comput. Phys. Commun. 217, 117–127. https://doi.org/10.1016/j.cpc.2017.03.002.
Tavakkol, S., Lynett, P., 2020. Celeris Base: an interactive and immersive Boussinesq-type nearshore wave simulation software. Comput. Phys. Commun. 248, 106966. https://doi.org/10.1016/j.cpc.2019.106966.
Terry, J.P., Oliver, G.J.H., Friess, D.A., 2016. Ancient high-energy storm boulder deposits on Ko Samui, Thailand, and their significance for identifying coastal hazard risk. Palaeogeography, Palaeoclimatology, Palaeoecology 454, 282–293. https://doi.org/10.1016/j.palaeo.2016.04.046.
UNESCO, 2012. Exercise Caribe Wave/Lantex 13: a Caribbean Tsunami Warning Exercise, 20 March 2013; Volume 1: Participant Handbook, vol. 2. final report.
Uuemaa, E., Ahi, S., Montibeller, B., Muru, M., Kmoch, A., 2020. Vertical Accuracy of Freely Available Global Digital Elevation Models (ASTER, AW3D30, MERIT, TanDEM-X, SRTM, and NASADEM). Remote Sensing 12, 3482. https://doi.org/10.3390/rs12213482.
Vött, A., Brückner, H., Brockmüller, S., Handl, M., May, S.M., Gaki-Papanastassiou, K., Herd, R., Lang, F., Maroukian, H., Nelle, O., Papanastassiou, D., 2009. Traces of holocene tsunamis across the sound of Lefkada, NW Greece. Global Planet. Change 66, 112–128. https://doi.org/10.1016/j.gloplacha.2008.03.015. Quaternary sea-level changes : Records and Processes.
Watanabe, M., Goto, K., Roeber, V., Kan, H., Imamura, F., 2023. A Numerical Modeling Approach for Better Differentiation of Boulders Transported by a Tsunami, Storm, and Storm-Induced Energetic Infragravity Waves. Journal of Geophysical Research: Earth Surface 128 e2023JF007083. https://doi.org/10.1029/2023JF007083.
Watt, S., Jaffe, B., Morton, R., Richmond, B., Gelfenbaum, G., Coastal, 2010. Description of extreme-wave deposits on the northern coast of Bonaire, Netherlands Antilles. AGU Fall Meeting Abstracts.
Watts, P., Tappin, D.R., 2012. Geowave validation with case studies: accurate geology reproduces observations. In: Yamada, Y., Kawamura, K., Ikehara, K., Ogawa, Y., Urgeles, R., Mosher, D., Chaytor, J., Strasser, M. (Eds.), Submarine Mass Movements and Their Consequences, Advances in Natural and Technological Hazards Research. Springer, Netherlands, Dordrecht, pp. 517–524. https://doi.org/10.1007/978-94-007-2162-3_46.
Weiss, R., Diplas, P., 2015. Untangling boulder dislodgement in storms and tsunamis: is it possible with simple theories? G-cubed 16, 890–898. https://doi.org/10.1002/2014GC005682.
Young, R., Bryant, E., Price, D., 1996. Catastrophic wave (tsunami?) transport of boulders in southern New South Wales, Australia. Faculty of Science - Papers (Archive).
Zahibo, N., Pelinovsky, E., 2001. Evaluation of tsunami risk in the Lesser Antilles. Nat. Hazards Earth Syst. Sci. 1. https://doi.org/10.5194/nhess-1-221-2001.